A Unique Cellular Organization of Human Distal Airways and Its Disarray in Chronic Obstructive Pulmonary Disease

Samir Rustam[1,*], Yang Hu[2,*], Seyed Babak Mahjour[1], Scott H. Randell[3], Andre F. Rendeiro[2], Hiranmayi Ravichandran[2], Andreacarola Urso[4], Frank D'Ovidio[4], Fernando J. Martinez[1], Bradley Richmond[5,6], Vasiliy Polosukhin[5], Jonathan A. Kropski[5,6], Timothy S. Blackwell[5,6], Olivier Elemento[2], and Renat Shaykhiev[1,**]

[1]Department of Medicine, Division of Pulmonary and Critical Care Medicine, Weill Cornell Medical College, New York, NY
[2]Caryl and Israel Englander Institute for Precision Medicine, Department of Physiology and Biophysics, Weill Cornell Medical College, New York, NY
[3]Marsico Lung Institute, The University of North Carolina at Chapel Hill, Chapel Hill, NC
[4]Department of Surgery, Columbia University Medical Center, New York, NY
[5]Department of Veterans Affairs Medical Center, Nashville, TN
[6]Department of Medicine, Vanderbilt University, Nashville, TN

[*]Co-first authors

[**]Corresponding author. E-mail: res2003@med.cornell.edu

Abstract

In the human lung, terminal bronchioles (TBs), the most distal conducting airways, open to respiratory bronchioles (RBs) that lead to the alveolar region where gas exchange takes place. This transition occurs in pulmonary lobules, lung tissue units supplied by pre-TBs, which give rise to TBs. Accumulating evidence suggests that remodeling and loss of pre-TBs and TBs underlies progressive airflow limitation in chronic obstructive pulmonary disease (COPD), the third leading cause of death worldwide. Understanding the nature of these changes at the single-cell level has so far been limited by poor accessibility of pre-TBs and TBs. Here, we introduce a novel method of region-precise airway dissection, which enables capture of the entire anatomical continuum of peripheral airways, from pre-TBs to RBs, and the associated alveolar region within the lobule. This approach allowed us to identify terminal airway-enriched secretory cells (TASCs), a unique epithelial cell population of distal airways expressing secretoglobin 3A2 (SCGB3A2) and/or surfactant protein B (SFTPB). TASCs were enriched in TBs, particularly, in areas of TB-RB transition and exhibited an intermediate, broncho-alveolar molecular pattern. TASC frequency was markedly decreased in pre-TBs and TBs of COPD patients compared to those in non-diseased lungs, accompanied by changes in cellular composition of vascular and immune microenvironments. *In vitro* regeneration assays identified basal cells (BCs) of pre-TBs and TBs as a cellular origin of TASCs in the human lung. Generation of TASCs by these region-specific progenitors was suppressed by IFN-γ signaling that was augmented in distal airways of COPD patients. Thus, altered maintenance of region-specific cellular organization of pre-TBs and TBs represents a key component of distal airway pathology in COPD.

52 **Introduction**

53 Distal airways, also known as "small airways" or "bronchioles" because of their small
54 size (diameter <2 mm), constitute peripheral segments of the tracheobronchial tree. Terminal
55 bronchioles (TBs), the most distal conducting airways, transition to respiratory bronchioles
56 (RBs), which mark the beginning of the respiratory zone and lead to the alveolar region, where
57 gas exchange takes place[1]. This transition occurs in secondary pulmonary lobules ("lobules"),
58 lung units, each supplied by an individual secondary lobular bronchiole, or pre-TB, which
59 bifurcates inside the lobule to give rise to TBs[2,3]. Accumulating evidence generated in computed
60 tomography imaging studies indicates that remodeling and loss of distal airways, including pre-
61 TBs and TBs, underlie progressive and irreversible airflow limitation in chronic obstructive
62 pulmonary disease (COPD)[4–11], a major smoking-related lung disorder and the 3rd leading cause
63 of death worldwide[12]. The nature of these structural alterations remains poorly understood at the
64 cellular level, in part, due to poor accessibility of pre-TBs and TBs and limited knowledge about
65 specific aspects of their cellular organization and homeostasis.

66 In this study, we established the method of a region-precise dissection of human distal
67 airways at the resolution of pre-TBs and lobules and characterized their cellular organization at
68 the single-cell level. This method enabled us to identify terminal airway-enriched secretory cells
69 (TASCs), a unique epithelial cell state of distal airways. TASCs were marked by expression of
70 secretoglobin 3A2 (SCGB3A2) and/or surfactant protein B (SFTPB), exhibited a molecular
71 pattern associated with the transition of conducting airways to the respiratory zone, and were
72 maintained by basal cells residing in pre-TBs and TBs. Loss of TASCs was observed in pre-TBs
73 and TBs of COPD patients paralleled by changes in the cellular composition of region-specific
74 vascular and immune microenvironments. These data suggest that altered maintenance of region-
75 specific cellular heterogeneity of pre-TBs and TBs underlies distal airway remodeling in COPD.

Results

Anatomical Landmarking of Human Distal Airways

Based on the anatomical definition of a pre-TB as the last macroscopically recognizable segment along the bronchial pathway that leads to secondary pulmonary lobule[2,3], we developed the method of a region-precise distal airway dissection, which regards pre-TBs as the boundary between pre-terminal (pre-T) and terminal (T) airways **(Fig. 1A)**. The pre-T-region included pre-TBs and 3-4 generations of airways proximal to pre-TBs, the T-region included macroscopically inseparable segments distal to pre-TBs (TBs, RBs, alveolar ducts and alveoli) within the lobule, whereas cartilaginous bronchi represented proximal (P) airways **(Fig. 1B** and **Fig. S1)**. The natural distribution of the landmark tissue elements was preserved in isolated samples: a) airway surface epithelium (ASE) with basal, ciliated and secretory cells; b) stroma with smooth muscle and vessels; c) submucosal glands (SMGs) and cartilage in P-airways; d) alveolar attachments in pre-T- and T-regions, and e) TBs, RBs, alveolar ducts and alveoli in T-region **(Fig. 1C-1E)**.

Cellular Diversity along the Bronchoalveolar Axis

To systematically assess cellular heterogeneity along the P-T airway axis, transcriptomes of 111,412 single cells isolated from airway regions of 17 donors (11-67 yrs old; **Table S1**), including P-airways of 5 donors without lung disease ("normal lung"), pre-T-region of 12 normal lung donors and 5 donors with COPD, and T-region of 7 normal lung donors, were analyzed by single-cell RNA-sequencing (scRNA-seq). By performing UMAP clustering and inspecting marker genes in identified clusters, 48 cell types and subtypes were identified **(Fig. 2A** and **Fig. S2; Table S2)**. Hierarchical clustering classified these cell groups into three superfamilies: 1) epithelial, including ASE, SMG and alveolar (AT) cell families, 2) structural, including stromal and endothelial (En) cell families, and 3) immune, including myeloid and lymphoid cell families **(Fig. 2B)**.

100 *Epithelial cells.* ASE was the most diverse family of epithelial cells. It included a spectrum of
101 cell states reflecting a trajectory of airway epithelial differentiation from undifferentiated cells
102 (*S100A2*$^{+}$ *KRT17*$^{+}$), including basal cells (BCs; *KRT5*^{hi} *KRT15*^{hi}), stem cells of ASE[13,14], and
103 intermediate cells (ICs, *SERPINB3*^{hi} *ALDH3A1*^{hi}), to two major differentiated ASE cell types,
104 i.e., secretory (S) and ciliated (C) cells **(Fig. 2B, C)**. S-cells (*SCGB1A1*^{hi} *SCGB3A1*^{hi}*)* included
105 common S-cells (S1), mucus-producing cells (S-Muc, *TFF3*^{hi} *MUC5AC*^{hi} *MUC5B*^{hi} *VMO1*^{hi}*)*,
106 and a distinct subset of cells expressing *SCGB3A2* and *SFTPB*, which formed a "bridge" cluster
107 between S- and type 2 alveolar epithelial (AT2) cells **(Fig. 2A, C)**. Cells in this intermediate
108 cluster were present almost exclusively in pre-T and T-regions, being enriched in the latter (see
109 below), and, therefore, were named "terminal airway-enriched secretory cells" (TASCs).
110 C-cells (*CAPS*$^{+}$ *FOXJ1*$^{+}$) included major (C1) and secretory-like (C-s; *SAA1*$^{+}$ *SAA2*$^{+}$)
111 subsets. Two clusters were found between C- and S-cells (S-C-intermediate; SCI cells; **Fig. 2A,**
112 **B)**. One of these SCI clusters expressed markers of deuterosomal precursors of C-cells (*CCNO,*
113 *CDC20B, HES6*)[15] and was termed "pre-ciliated" (p-C) cells. Another co-expressed C, S1 and S-
114 Muc marker genes, and, consistent with recently reported findings[15–17], was named "S-C hybrid"
115 (H) cells. Our analysis also captured rare ASE cell types - ionocytes (Ion, *ATP6V0B*$^{+}$ *FOXI1*$^{+}$
116 *TMEM61*$^{+}$ *CFTR*$^{+}$)[18,19] and neuroendocrine (NE) cells (*CHGA*$^{+}$ *GRP*$^{+}$) (**Fig. 2C**).
117 The SMG family included glandular (G; *AZGP1*^{hi}) mucous (G-Muc; *MUC5B*$^{+}$ *BPIFB2*$^{+}$)
118 and serous (G-Ser; *LYZ*^{hi} *LTF*^{hi} *PRR4*^{hi}) cells[20], and myoepithelial (ME) cells (*KRT5*$^{+}$ *KRT14*$^{+}$
119 *ACTA2*$^{+}$, SMG stem cells[21,22]) **(Fig. 2B, C)**. The AT family included type 1 (AT1; *AGER*$^{+}$) and
120 type 2 (AT2; *SFTPC*$^{+}$) alveolar epithelial cells **(Fig. 2C)**. Consistent with their intermediate
121 clustering between S- and AT2 cells, TASCs, in addition to common S-cell genes, expressed a
122 set of genes enriched in AT2 cells (*SFTPB, RNASE1, CYB5A)*, but, in contrast to the latter, did
123 not express *SFTPC*, the obligatory AT2 cell marker **(Fig. 2C**; and below**)**.

124 *Structural cells*. The stromal family included chondrocytes (Cr; *SNORC*$^{+}$ *CHI3L1*$^{+}$), fibroblasts
125 (Fb; *FBLN1*$^{+}$ *DCN*$^{+}$), smooth muscle cells (SM; *ACTA2*$^{+}$ *TAGLN*$^{+}$) and pericytes (*PDGFRB*$^{+}$
126 *COX4I2*$^{+}$) **(Fig. 2C)**. Fb included four subsets: common (Fb1), *CCL19*$^{+}$ (Fb2; included *SFRP2*$^{+}$
127 adventitial Fb[23]), matrix (Fb3, *ELN*^{hi} *COL1A1*^{hi} *MMP2*^{hi}; contained *ACTA2*$^{+}$ myoFbs[24,25]), and
128 Fb4 (contained *GPC3*$^{+}$ *FGFR4*$^{+}$ *VEGFD*$^{+}$ alveolar Fbs[23]). SM included SM1 and SM2 clusters
129 expressing markers of vascular SM (*ADIRF*, *NOTCH3*, *PDGFRB*)[23] and SM3 (*DES*$^{+}$ *TPM2*$^{+}$
130 *CNN1*$^{+}$, airway SM markers[23]) **(Fig. 2C)**. A distinct group of cells clustered among stromal cells
131 and expressed markers of neuronal and glial/Schwann cells (*CDH19, GPM6B, MPZ, NRXN1*)
132 and, therefore, was annotated as glial/Schwann cells (Gli; **Fig. 2B**, **C**). The endothelial (En) cell
133 family (*CLDN5*^{hi} *CDH5*$^{+}$) included arterial (En-a; *IGFBP3*$^{+}$ *GJA5*$^{+}$ *DKK2*$^{+}$*)*, common capillary
134 (En-c1; *FCN3*$^{+}$ *CA4*$^{+}$), a distinct cluster of En-capillary cells expressing markers of recently
135 described alveolar capillary aerocytes[23] (En-ca; *HPGD*, *EDNRB*, *IL1RL1*), venous (En-v;
136 included cells expressing markers of the fenestrated endothelium *ACKR1* and *PLVAP*[23]), En-sm
137 co-expressing En- and SM markers, and lymphatic (En-l; *CCL21*$^{+}$ *MMRN*$^{+}$*)* **(Fig. 2C)**.

138 *Immune cells.* Myeloid cells included neutrophils (Neu; *S100A8*^{hi} *IFITM2*^{hi} *CXCL8*^{hi} *CSF3R*$^{+}$)[23],
139 mast cells (MC; *TPSB2*$^{+}$ *TPSAB1*$^{+}$)*,* a spectrum of cellular states representing the mononuclear
140 phagocyte system - from monocytes (Mon; *IL1B*$^{+}$ *EREG*$^{+}$) to macrophages (M; *CD163*^{hi} *CD68*^{hi})
141 and dendritic cells (DCs). The latter included conventional, or myeloid, DCs (cDCs) marked by
142 high expression of the *HLA* family genes, and plasmacytoid (pDCs; *IL3RA*$^{+}$ *IRF7*$^{+}$) **(Fig. 2B**, **C)**.
143 Three M-subsets were identified: inflammatory (M1; *SPP1*$^{+}$ *CCL3*$^{+}$), non-inflammatory (M2;
144 *MSR1*$^{+}$ *FABP4*$^{+}$ *CCL18*$^{+}$), which resembled classically (M1) and alternatively (M2) activated
145 macrophage polarization states[26], both expressing *MARCO*, a marker of embryonically derived
146 lung-resident macrophages[27,28], and intermediate (M1-2) state **(Fig. 2C)**.

147 The lymphoid family included B (*MS4A1*$^{+}$), plasma (PC; *JCHAIN*$^{+}$ *MZB1*$^{+}$), T (*CD3D*$^{+}$)
148 and NK (*GNLY*^{hi} *NKG7*^{hi}) cells **(Fig. 2C)**. Multiple T-cell subsets were identified, including
149 those expressing markers of central memory and naïve T cells (Tcn; *CCR7*$^{+}$ *IL7R*$^{+}$ *LTB*$^{+}$ *SELL*$^{+}$),
150 T-cells expressing interferon (IFN)-response genes (T-ifn, *IFIT1*$^{+}$ *IFIT2*$^{+}$ *ISG15*$^{+}$*),* two CD8^{+} T
151 cell-enriched subsets - resident-memory (Trm; *CXCR6*$^{+}$ *CCL5*$^{+}$) and "common" CD8^{+} T cells
152 (CD8-T1), and T-cells co-expressing NK cell markers (T-NK; *GNLY*$^{+}$ *NKG7*$^{+}$)[29–31] **(Fig. 2C)**.
153 *Regional Heterogeneity of Epithelial Cells along the Bronchoalveolar Axis*
154 SMG cells were uniquely enriched in P-airways, whereas AT cells were found only in
155 pre-T and T-regions **(Fig. 3A)**, consistent with unique histological organization of these regions
156 **(Fig. 1D; Fig. S3)**. Undifferentiated ASE cells (BCs and ICs) were most abundant in P-airways
157 (43% of ASE cells *vs* <10% in pre-T and T; p<0.004), largely due to enrichment of ICs in P-
158 airways **(Fig. 3A, B; Table S3)**, where *SERPINB3*$^{+}$ ICs contributed to the pseudostratified ASE
159 pattern typical for P-airways **(Fig. S3A)**. The overall frequency of secretory-ciliated intermediate
160 (p-C and H) cells was higher in pre-T and T-airways (8-10% of ASE cells *vs* 1.4% in P; p<0.02;
161 **Fig. 3B)**. The overall frequency of S- and common S1-cells was similar across the regions **(Fig.
162 3A, B)**. However, TASCs, a novel S-cell population identified in this study, were found almost
163 exclusively in distal (pre-T and T-regions) with significant enrichment in the T-region (p<0.02 *vs*
164 pre-T; **Fig. 3B; Table S3**), the basis for their designation as T-airway-enriched S-cells.
165 *Terminal Airway-enriched Secretory Cells (TASCs)*
166 To comprehensively characterize the molecular phenotype of TASCs, we compared their
167 transcriptomes to those of their closest clustering neighbors - other ASE S- (S1 and S-Muc) cells
168 and AT2 cells **(Fig. 3C**, **D)**. Consistent with their intermediate clustering position, between S-
169 and AT2 cells, TASCs exhibited a transitional molecular pattern integrating features of these cell
170 types yet were distinct from each of them **(Fig. 3C)**. Compared to other ASE S-cells, TASCs had

171 significantly higher expression of TASC markers *SCGB3A2* and *SFTPB*, and a distinct set of
172 genes highly expressed in AT cells, including *RNASE1*, *SFTPA2*, *CYB5A, HOPX* and *SFTPA1*
173 **(Fig. 3C, D)**. Compared to AT2 cells, TASCs had significantly higher expression of airway S-
174 cell markers *SCGB1A1*, *SCGB3A1* and *BPIFB1*, but lower expression of AT2 marker genes
175 *SFTPC*, *SFTPA1* and *SFTPA2*. Notably, *SCGB3A2* and *MGP* were expressed in TASCs higher
176 than in both S- and AT2 cells **(Fig. 3C, D; Table S4)**. TASCs were *bona fide* single cells, as
177 determined by a rigorous doublet detection protocol[32] **(**see **Supplemental Methods)**.
178 Consistent with scRNA-seq data, immunofluorescence (IF) analysis of normal lung tissue
179 samples confirmed that TASCs, identified as ASE cells containing secretoglobin SCGB3A2 and
180 surfactant protein SFTPB, are unique to distal airways **(Fig. 3E, F; Fig. S4)**. IF analysis of 24
181 normal lung tissue samples (>80,000 ASE cells; **Table S5)** determined that $SCGB3A2^{+}$ TASCs
182 constitute 8% and 23% of ASE cells in pre-TBs and TBs, respectively ($p<0.0002$ TB *vs* pre-TB)
183 and >40% in the transitioning simple columnar-to-cuboidal epithelium at TB-RB junctions
184 ($p<10^{-4}$ *vs* TB overall; **Fig. 3G**). SFTPB marked a broader subset of TASCs (~16% of ASE cells
185 in pre-TBs; ~33% in TBs; $p<0.0003$, TB *vs* pre-TB; ~54% in TB-RB junction areas; $p=0.0002$ *vs*
186 TB overall; **Fig. 3H)**. Compared to a dome-shaped appearance of TASCs in the pseudostratified
187 epithelium of pre-TBs and proximal aspects of TBs, in TB-RB junctional areas, where the
188 epithelium transitioned to a simple columnar-to-cuboidal pattern, TASCs acquired a cuboidal
189 shape typical for the transitional cuboidal epithelium of RBs[33] **(Fig. S4A-B)**.
190 The molecular pattern of TASCs changed along the pre-TB-RB axis. In pre-TBs, 44.2%
191 of TASCs co-expressed SCGB1A1, a marker of common S-cells, compared to 30.5% of TASCs
192 in TBs ($p<0.03$) and only 5.5% in TB-RB junctional areas ($p<10^{-5}$ *vs* TB overall; **Fig. 3I**). At the
193 single-cell mRNA level, TASCs in the T-region showed significantly higher expression of
194 *SFTPA2* compared to those in pre-T airways **(Fig. S5)**, but in contrast to AT2 cells, which also

195 expressed this gene, TASCs were largely negative for *SFTPC* **(Fig. 3J)**. As shown earlier[34], a
196 subset of SMG cells were SCGB3A2$^+$, but they did not express *SFTPB* or *SCGB1A1* **(Fig. 3J;**
197 **Fig. S3B and S4)** and, based on their transcriptome profiles, clustered separately from TASCs
198 **(Fig. 2A)**. Thus, TASCs represent a distinct subset of S-cells unique to distal airways and
199 enriched in areas of TB-RB transition.

200 *Regional Heterogeneity of Structural and Immune Cells*

201 Distribution of structural cells showed differences along the P-T axis, with significantly
202 higher frequency of endothelial (En)-cells in the T-region **(Fig. 3K)**. Among stromal cells,
203 chondrocytes, as expected, were found in cartilaginous P-airways, fibroblasts were most frequent
204 in pre-T and less frequent in P-airways **(Fig. 3L)**. Among fibroblasts, Fb2 (*CCL19*$^+$) were most
205 frequent in the P-region, whereas proportions of Fb3 and Fb4 increased along the P-T axis
206 **(Table S3)**. Pericytes also increased in frequency along this axis **(Fig. 3L**). By contrast, the
207 frequency of Gli-cells declined along the P-T axis from 2.4% of stromal cells in P-airways to
208 1.1% in pre-T ($p<0.05$ *vs* P) and 0.3% in T-region ($p=0.0057$ *vs* P+pre-T; **Fig. 3L)**. Among
209 endothelial cells, capillary (En-c1 and En-ca) cells were significantly enriched in the T-region
210 ($p<0.0003$ *vs* other regions), whereas the proportion of En-v cells, representing venous and
211 fenestrated endothelium, was highest in P-airways ($p=0.00125$ *vs* other regions) **(Fig. 3M)**. The
212 frequency of endothelial lymphatic (En-l) cells was highest in pre-T-region **(Fig. 3M)**.

213 Within the immune cell superfamily, the distribution of myeloid and lymphoid cells
214 showed opposite trends along the P-T axis, with the trend of a higher proportion of lymphoid
215 cells in P-airways **(Fig. 3N)**. Among lymphoid cell types, B, Tcn, CD8$^+$ (Trm + CD8$^+$T1)
216 showed a higher frequency in P-airways, whereas NK cells were more frequent in pre-T and T-
217 regions **(Fig. 3O)**. The total frequency of cells of the mononuclear phagocyte system (Mon, M,
218 DCs) in pre-T and T regions was higher compared P-airways **(Fig. 3O; Table S3)**.

219 *Altered Region-specific Cellular Composition of Distal Airways in COPD*

220 Pre-T airways isolated by our method included pre-TBs and more proximal bronchioles
221 with a luminal diameter <2 mm **(Fig. 1A)** and, thus, represented small airways known to be
222 affected in COPD[4–8]. To determine cellular basis of disease-related pathologic changes in these
223 airways at the single-cell level, we compared the cellular composition of pre-T samples isolated
224 from 5 subjects with COPD and 12 donors without lung disease ("normal" lungs) using scRNA-
225 seq analysis. Whereas the overall distribution of major cell types was comparable in both groups
226 **(Fig. 4A)**, disease-related changes preferentially involved cell populations, which contributed to
227 physiological cellular heterogeneity along the airway axis. This included the loss of TASCs and
228 En-c cells normally enriched in the distal airway region, and increased proportions of Gli and
229 CD8-T1 cells normally enriched in P-airways. There was also a dramatic, 4.7-fold increase in the
230 frequency of MCs in pre-T airways of COPD patients compared to normal. Proportions of these
231 cells were significantly different in pre-T airways of COPD patients compared to normal lung
232 donors among all captured cells **(Fig. 4A)** and within corresponding superfamilies **(Fig. 4B)**.

233 To identify disease-related molecular changes in specific cell types and subtypes, we
234 compared gene expression profiles of specific cell populations captured in scRNA-seq analysis
235 of pre-T airways of COPD patients and normal lung donors **(Fig. 4C)**. The highest numbers of
236 up-regulated genes in COPD *vs* non-diseased pre-T samples were observed in MCs (2716 genes),
237 BCs (1605 genes), Fb1 (1641 gene), CD8-T1 (1560 genes), Gli (1302 genes), M2 (1151 gene)
238 and T-NK (1074 genes). The highest numbers of suppressed genes in COPD compared to normal
239 pre-T samples were found in En-ca subset of capillary En-cells (1072 genes), TASCs (831 gene)
240 and common S (S1) cells (648 genes) **(Fig. 4C; Table S6)**. Thus, altered cellular composition of
241 pre-T airways in COPD subjects is paralleled by changes in transcriptional states of a distinct set
242 of cell populations, including those contributing to the region-specific pattern of distal airways.

243 To determine most prevalent molecular changes occurring within the ASE compartment
244 of COPD pre-T airways, we performed pseudobulk analysis of transcriptional profiles of pre-T
245 ASE cells of COPD subjects compared to those from normal lung donors using scRNA-seq data
246 described above. Among top down-regulated genes were common S (S1) cell markers, including
247 *SCGB1A1* and *SCGB3A1*, and markers of TASCs *SCGB3A2* and *SFTPB* **(Fig. 4D)**. Thus, loss of
248 secretory differentiation features, both general and region-specific, represents a major disease-
249 related transcriptional phenotype of ASE in COPD pre-T airways. Among the genes up-regulated
250 in ASE of COPD pre-T airways were those related to the *HLA* family (*HLA-DRB5* and *HLA-B*)
251 and markers of undifferentiated ASE cells, BCs and ICs, *ALDH3A1*, *KRT6A*, *KRT5, KRT17* and
252 *S100A2*) **(Fig. 4D; Table S7)**. Immune signaling pathways, including those related to IFN-γ
253 signaling, were identified as the top biological categories enriched among genes up-regulated in
254 ASE of COPD *vs* normal pre-T-airways **(Fig. 4E; Table S8)**.
255 In agreement with scRNA-seq data, quantitative IF analysis, in which >50,000 ASE cells
256 lining pre-TB/TBs in lung tissue samples of 11 COPD subjects were assessed comparatively to
257 non-diseased samples described above, revealed significantly reduced frequency of $SCGB3A2^+$
258 and $SFTPB^+$ TASCs in pre-TBs and TBs of COPD subjects **(Fig. 4F; Table S5)**. Particularly
259 dramatic loss of $SCGB3A2^+$ TASCs in the lungs of COPD patients was in pre-TBs (on average,
260 1.5% of ASE cells *vs* 8.0% in non-diseased donors; $p<0.005$). The average frequency of $SFTPB^+$
261 TASCs in the ASE of COPD pre-TBs was 6.3% *vs* 15.9% in normal lung donors ($p<0.007$) **(Fig.
262 4F)**. Whereas in non-diseased lungs, TASCs were detected in all inspected pre-TBs (based on
263 SFTPB positivity) and $SCGB3A2^+$ TASCs were found in >92% of them, no single TASC could
264 be detected in 55.4% and 10.9% of pre-TBs in COPD subjects, based on SCGB3A2 and SFTPB
265 positivity, respectively ($p<0.05$ *vs* non-diseased donors; **Fig. 4G**).
266

267 The average frequency of TASCs in TBs of COPD subjects was about two times lower
268 compared to that in non-diseased lungs based on both SCGB3A2 and SFTPB staining ($p<0.003$
269 for both markers; **Fig. 4F**). Whereas >99% of inspected TBs in non-diseased lungs contained
270 SCGB3A2$^+$ TASCs, this subset of TASCs was not detected in 26.9% of TBs of COPD subjects
271 **(Fig. 4G)**. There was also significantly lower proportion of TBs containing TASCs at frequency
272 of >10% of ASE cells in COPD compared to non-diseased lungs, based on both SCGB3A2 and
273 SFTPB expression **(Fig. 4G)**. In TB-RB junction areas, where TASCs were most abundant in
274 both groups, differences in their frequency between COPD and normal lungs were less dramatic,
275 but still significant for SCGB3A2$^+$ TASCs **(Fig. 4F; Table S5)**. A remarkable heterogeneity was
276 noted with regard to the extent of TASC loss in the lungs of different COPD patients and/or in
277 different pre-TB/TBs regions of the same patient lungs **(Fig. 4F-H)**. In some COPD samples,
278 TASCs were preserved in a subset of pre-TB/TBs but undetectable in other distal airways of the
279 same anatomical category **(Fig. 4H; Fig. S6A-B)**.
280 Notably, common SCGB1A1$^+$ S-cells could still be detected in a subset of pre-TBs/TBs
281 of COPD patients, where TASCs were absent **(Fig. 4H; Fig. S6B)**, indicating that loss of TASCs
282 in COPD occurs earlier and is independent from changes in common S (S1) cell differentiation
283 in these airways. In support of the latter possibility, based on quantitative IF analysis, there was
284 no significant change in the frequency of SCGB1A1$^+$ S1-cells in pre-TBs and TBs of COPD
285 subjects, and no significant correlation was observed between loss of TASCs and changes in the
286 overall SCGB1A1$^+$ S1-cell frequency in pre-TBs and TBs **(Fig. S7)**. Further, no significant
287 change was detected in the frequency of TASCs in pre-TBs and TBs of smokers without lung
288 disease compared to nonsmokers **(Fig. S8)**, suggesting that loss of TASCs in distal airways of
289 COPD patients represents a disease-related phenotype rather than a common response of distal
290 airways to cigarette smoking, the major risk factor for COPD[12].

291 *Distal Airway BCs are Cellular Origin of TASCs*

292 To determine the biological basis of regional heterogeneity of epithelial cells along the
293 proximal-distal airway axis, we focused on airway BCs, stem cells of ASE[13,35]. We hypothesized
294 that, as local epithelial progenitors[36], BCs maintain a regional memory, an intrinsic capacity to
295 regenerate epithelium with cellular composition specific to the region of their residence. To test
296 this hypothesis, we isolated BCs from proximal (P) and distal (D: pre-T) airways of 6 donors
297 without lung disease **(Table S10)** and compared their differentiation potential in the air-liquid
298 interface (ALI) model. In this model, BCs after establishing a confluent monolayer generate
299 differentiated airway epithelium within few weeks upon apical exposure to air[37] **(Fig. 5A)**.
300 Paired comparative analysis of transcriptomic profiles of epithelia generated by P- and D-airway
301 BCs after 18 days of ALI culture identified 2,005 DEGs, including 888 and 1117 genes with
302 significantly higher expression in epithelia produced by P- and D-airway BCs, respectively
303 **(Table S11)**. Among the genes uniquely up-regulated in epithelia generated by D-airway BCs
304 were *SFTPB, SCGB3A2, SFTA2, RNASE1* and *SFTPA2* **(Fig. 5B)**, i.e., genes, which as described
305 above, were uniquely expressed or enriched in TASCs *in vivo*. Indeed, 21.3% of genes most
306 robustly up-regulated in D- *vs* P-airway BC-derived epithelia (log2FC >1) were genes that
307 distinguished TASCs from other ASE cells *in vivo* **(Fig. 5C)**. Consistent with these data, IF
308 analysis identified SCGB3A2^{+} cells in differentiated epithelia derived from D-airway BCs, but
309 not P-airway BCs **(Fig. 5D)**. By contrast, MUC5AC^{+} mucus-producing S-cells were found more
310 frequently in epithelia derived from P-airway BCs **(Fig. 5D)**, although this was not a consistent
311 region-specific feature of P-airway epithelium at the gene expression level. Together, these data
312 suggest that the ability to generate TASCs is a unique, region-specific feature of D-airway BCs,
313 and even after isolation of BCs from their *in vivo* microenvironment, these progenitors continue
314 to maintain an intrinsic memory of region-specific differentiation.

315 To evaluate the dynamics of distal airway epithelial differentiation at the single-cell level,
316 epithelia generated at days 0, 3, 7, 14 and 28 of ALI culture of the same D-airway BC sample
317 were profiled using scRNA-seq. A total of 36,321 single cells were captured in this analysis
318 **(Table S12)**. As expected, cellular diversity progressively increased during BC differentiation
319 **(Fig. 5E, F)**. At ALI-day 0, >99% of cells were BCs, which included two subsets: BC1, which
320 expressed typical BC markers, and S-like BCs (BC-s), which differed from BC1 by expression of
321 S-cell-related genes, e.g., *SCGB1A1* and *MUC5B* (see markers of all cell types in **Table S13**). At
322 ALI-day 3, in addition to BCs, which at this stage included 3 subsets: BC1, proliferating (BC-p),
323 and matrix (BC-m) showing high expression of extracellular matrix-related genes (e.g., *MMP1,*
324 *LAMC2*, *MMP10* and *LAMB3*; **Table S13)**, several other cell types emerged. They included IC1
325 (*SERPINB3*^{high}) and squamous ICs (IC-sq; *KRT6A*$^{+}$ *SPRR1B*$^{+}$), which together constituted 53%
326 of cells at ALI-day 3; pre-ciliated (p-C) cells (*CCNO*$^{+}$ *HES6*$^{+}$; ~7% of cells at this time-point),
327 initial ciliated cells (C1), Ion, and rare tuft-like cells (TLCs) co-expressing markers of Ion, NE
328 and brush, or tuft cells[18,19] **(Fig. 5E, F** and **Fig. S9)**. At ALI-day 7, proportions of BCs and ICs
329 reduced, while S1-cells *(SCGB1A1*^{high}*)*, which emerged at this time-point as a cluster extending
330 further from ICs on the BC differentiation trajectory, constituted ~56% of all cells. Also at day 7,
331 TASCs emerged as an extension of the S-cell cluster further distant from BCs, and the frequency
332 of C-cells, containing C1 and C-s subsets, increased to 5% **(Fig. 5E, F; Table S12)**. Frequencies
333 of C-cells and TASCs increased to 17% and 3%, respectively, by ALI-day 14 and further to 30%
334 and 22% by ALI-day 28 **(Fig. 5F)**. The overall cellular composition of epithelium produced by
335 D-airway BCs after 28 days of differentiation on ALI resembled that observed in D-airways *in*
336 *vivo*, with major differentiated cell types (C- and S-, including TASCs) constituting together
337 >80% of ASE cells **(Fig. 5E-F; Tables S3 and S12)**.

338 Remarkable similarity of marker gene profiles of cell types generated by D-airway BCs
339 *in vitro* to those *in vivo*, measured for each ASE cell type as an overlap of DEGs identified for
340 the same ASE cell type *in vitro* and *in vivo* using identical criteria (FDR<0.05; log2 fold-change
341 >0.5 *vs* other ASE cells), was noted. The highest degree of similarity in this regard was observed
342 for C1-cells, whose *in vitro* markers overlapped with 91.3% of DEGs distinguishing these cells
343 from other ASE cells *in vivo,* followed by C-s (56.4%), p-C (48.8%), BC (47.0%), IC (38.9%),
344 TASC (35.9%) and Ion (28%) **(Fig. 5G; Table S14)**. Compared to common secretory (S1) cells,
345 TASCs generated in the same ALI culture displayed significantly higher expression of 84 genes,
346 40 of which were among those identified in a similar comparison of TASCs and S1 cells *in vivo*,
347 including *SCGB3A2* and *SFTPB* **(Fig. 5H; Table S15)**. Together, these data indicate that distal
348 airway BCs are region-specific epithelial progenitors capable for regenerating TASCs in this
349 anatomical region.

350 *IFN-γ Inhibits TASC Regeneration by Distal Airway BCs*

351 Based on our *in vitro* data showing the role of distal airway BCs as the cellular origin of
352 region-specific ASE including TASCs, and our *in vivo* scRNA-seq data showing the enrichment
353 of IFN-γ signaling pathway in COPD distal ASE **(Fig. 4E)**, we hypothesized that loss of TASCs
354 in COPD is mediated by augmented IFN-γ signaling in BCs residing in distal airways. Consistent
355 with earlier studies[4,38,39], the frequency of $CD8^+$ T cells, one of the major *IFNG*-expressing cell
356 populations in the human lung **(Fig. 2C and Fig. S10A)**, was significantly greater in distal (pre-
357 T) airways of COPD patients compared to those in normal lung donors **(Fig. 4B)**. Imaging
358 CyTOF analysis mapped $CD8^+$ cells to sub- and intraepithelial domains of pre-TBs and TBs in
359 close proximity to BCs and ICs **(Fig. S10B)**, which, based on scRNA-seq data, expressed IFN-γ
360 receptor genes *IFNGR1* and *IFNGR2 in vivo* and *in vitro* **(Fig. S10C)** and, thus, represent
361 potential target cell populations for IFN-γ in distal airways.

362 We tested this hypothesis by evaluating the differentiation of BCs isolated from distal
363 airways in the presence or absence of IFN-γ added from the basolateral side of ALI culture to
364 enable the access to BCs during at least 10 days between ALI days 0 and 40 **(Fig. S10D)**. In 5
365 independent experiments, stimulation with IFN-γ induced IFN-γ-response genes *MX1*, *IFIT1* and
366 *CXCL10* in BC-derived epithelia **(Fig. 5I** and **S10D)**, suggesting that BCs can operate as IFN-γ-
367 sensors and responders in human airways. This was accompanied by down-regulation of TASC
368 marker genes *SCGB3A2* and *SFTPB* in epithelia derived from IFN-γ-treated distal airway BCs
369 **(Fig. 5I)**. Although there was a trend of reduced expression of a common S-cell gene *SCGB1A1*
370 in IFN-γ-treated group, there was no consistent change in expression of the mucus-related gene
371 *MUC5B* and the ciliated cell marker *FOXJ1* in response to IFN-γ **(Fig. S10D)**. Thus, by acting
372 on distal airway BCs, IFN-γ inhibits the regeneration of non-mucous S-cells, predominantly
373 TASCs, by these progenitors, inducing the altered epithelial differentiation phenotype observed
374 in pre-T airways of COPD patients.

375 **Discussion**

376 In this study, using a novel, region-precise method of airway dissection, we assembled an
377 atlas of cellular heterogeneity along the proximal-distal axis of the human respiratory tree. Our
378 study captured 48 cell types and subtypes representing all histological elements along this axis.
379 A novel, anatomy-guided approach to distal airway dissection in our study, which regards
380 secondary lobular bronchioles, pre-TBs, the last macroscopically distinguishable segments along
381 the bronchial pathway[2], as anatomical landmarks for region-precise isolation of distal airways,
382 allowed us to characterize cellular organization of peripheral bronchioles at the single-cell level.
383 In our approach, pre-TBs served as the boundary between pre-terminal (pre-T) airways and the
384 terminal (T) bronchoalveolar region. While the former included pre-TBs and bronchioles leading

385 to them, the T-region harbored the entire continuum of microscopic anatomical segments, from
386 TBs to alveolar sacs, within secondary pulmonary lobules, known to be the functional and
387 structural lung units, each supplied by an individual pre-TB[2,3]. Such an approach allowed us to
388 systematically characterize, at single-cell resolution, gradual changes in cellular composition
389 occurring along the bronchoalveolar continuum of human lung.

390 One of the major findings of our study enabled by this region-precise dissection method
391 was the identification of terminal airway-enriched secretory cells (TASCs), a unique population
392 of epithelial cells specific to distal airways that expressed secretoglobin 3A2 (*SCGB3A2*) and/or
393 surfactant protein B (*SFTPB*). As their name implies, TASCs were enriched in terminal airway
394 segments, TBs, and, particularly, in TB-RB junction areas, where conducting airways transition
395 to the respiratory zone[1]. Consistent with their enrichment in this transitional region, TASCs
396 displayed an intermediate molecular pattern that integrated a distinct set of airway secretory and
397 alveolar type 2 cell (AT2) features and gradually changed as airways approached the respiratory
398 zone. In pre-TBs, >40% of TASCs expressed SCGB1A1, a marker of airway secretory (S)-cells,
399 and, similar to the latter, appeared as dome-shaped non-ciliated bronchiolar, or club, cells[40]. Yet,
400 compared to other S-cells, TASCs expressed *SCGB3A2* and *SFTPB* and a set of genes, including
401 *SFTPA2*, *HOPX* and *SFTPA1,* characteristic for AT2 cells[23]. In TB-RB junction areas, however,
402 >90% of TASCs did not express SCGB1A1 protein and were morphologically identical to
403 cuboidal cells of RBs[33,41]. Consistent with this, TASCs in T-airways up-regulated *SFTPA2*, a
404 gene coding for surfactant protein A, known to mark cuboidal cells of transitional epithelium of
405 RBs[33]. TASCs did not typically express *SFTPC*, the obligate marker of AT2 cells. Thus, TASCs
406 comprise a spectrum of epithelial states in the peripheral region of the respiratory tree gradually
407 changing as distal conducting airways transition to the respiratory zone, culminating in cuboidal
408 cells of RBs[33,41], which remained poorly characterized prior to this study.

409 A progressive increase in TASC abundance along the proximal-distal axis of the airway
410 tree was paralleled by changes in the distribution of several non-epithelial cell types contributing
411 to region-specific tissue microenvironments. Endothelial capillary cells, including recently
412 described alveolar capillary aerocytes[23], progressively increased in frequency as airways became
413 smaller and transitioned to the respiratory zone. By contrast, venous endothelial cells, including
414 those with features of the fenestrated endothelium, were most abundant in P-airways, likely
415 representing post-capillary venules of the bronchial vasculature serving as ports of leukocyte
416 entry into the bronchial mucosa or lymph nodes[42]. Glia/Schwann cells were most abundant in P-
417 airways and decreased in frequency along the proximal-distal axis, mirroring the density of
418 cholinergic innervation that regulates bronchoconstriction and mucus secretion from submucosal
419 glands in this anatomical region[20,43,44].
420 Our study also identified regional compartmentalization of immune cell niches along the
421 bronchoalveolar axis with reciprocal enrichment of lymphoid and myeloid cells in proximal (P)
422 and distal airway regions, respectively. B-cells and various T-cell subsets, such as central and
423 naïve, resident memory and common $CD8^+$-enriched T-cells, were more abundant in P-airways,
424 while cells of the mononuclear phagocyte family were overall more frequent in distal regions.
425 Such heterogeneity may govern region-specific host defense strategies in the respiratory tract,
426 with higher baseline adaptive immune potential, capable of post-infection memory, in P-airways,
427 more frequently exposed to pathogens[45], and reliance on innate immune potential of monocytes
428 and resident macrophages as a homeostatic defense strategy in distal airways and alveoli[28,46].
429 Many key aspects of region-specific cellular organization of distal airways identified in
430 our study showed an altered distribution in distal airways of patients with COPD, a disease, in
431 which progressive airflow obstruction develops due to remodeling of peripheral bronchioles,
432 from pre-TBs to RBs[4–8], i.e., those captured by our airway dissection method. Although various

433 aspects of this remodeling, including airway wall thickening, lumen narrowing, inflammation
434 and loss of small airways, have been extensively studied using micro-/computed tomography and
435 histologically[4–8], the cellular basis of these changes remains poorly understood. The region-
436 precise approach to peripheral airway analysis in our study allowed us to systematically identify
437 changes in cellular organization of distal airways in COPD at single-cell resolution.

438 Among the changes identified in COPD distal airways in our analysis was loss of TASCs,
439 which, as detailed above, represent a unique epithelial cell population of distal airways. In COPD
440 lungs, TASC frequency was reduced in all distal airway segments, from pre-TBs to TB-RB
441 junctions, with particularly dramatic loss in pre-TBs, where TASCs were on average about five
442 times less frequent than in non-diseased lungs. Loss of TASCs in COPD was not paralleled by
443 altered distribution of other airway surface epithelial cells in this anatomical region, including
444 common S- and ciliated cells, known to be affected by cigarette smoking, the major risk factor
445 for COPD[47]. Further, no significant difference in the frequency of TASCs was noted in distal
446 airways of healthy smokers compared to nonsmokers, suggesting that loss of TASCs in COPD
447 represents a disease-associated phenotype rather than merely a response to cigarette smoking.

448 In our previous study[48], down-regulation of *SCGB3A2* and *SFTPB*, markers of TASCs,
449 paralleled by acquisition of P-airway-like molecular pattern, was found in samples obtained by
450 bronchoscopy from the 10th-12th generation bronchi of COPD subjects and healthy smokers who
451 had a lower forced expiratory volume in one sec/forced vital capacity (FEV1/FVC) ratio, a
452 spirometric measure of airway obstruction, compared to other smokers. Thus, it is possible that
453 molecular changes in more proximal, bronchoscopically accessible small airways may precede
454 and predict loss of TASCs in pre-TBs and TBs (generations 15-16)[49] as COPD develops. Future
455 studies are needed to determine whether loss of TASCs in pe-TBs and TBs correlates with or
456 precedes loss of these airways known to occur relatively early during disease progression[4–8].

457 Loss of TASCs in distal airways in COPD was paralleled by changes in the composition
458 of non-epithelial cell populations contributing to the region-specific microenvironment in these
459 airways, including a dramatic reduction of capillary endothelial cells, particularly those with
460 features of capillary aerocytes[23], normally enriched along the proximal-distal airway axis. This
461 was reciprocated by an increased frequency of glial/Schwann cells and $CD8^+$-enriched T-cell
462 subsets, which in normal lungs were more abundant in proximal airways. Although the role of
463 Schwann cells in COPD is unknown, it is possible that higher abundance of these cells in distal
464 airways reflects increased density of sensory neurons potentially relevant to pathogenesis of
465 chronic cough and mucus hypersecretion in this disease[50,51]. The increased number of $CD8^+$ T
466 cells in distal airways of COPD patients has been observed in earlier studies[39]. Consistent with
467 higher expression of *INFG* in these $CD8^+$ T cells and earlier findings of augmented cytotoxic
468 IFN-γ- secreting T-cell responses in COPD[38], IFN-γ signaling was identified in our analysis as
469 the top biological pathway enriched in the distal airway epithelium of COPD patients.
470 Using an *in vitro* model of airway epithelial differentiation, our study identified distal
471 airway BCs as region-specific progenitors harboring "regional memory", an intrinsic program
472 that enables these cells to regenerate region-specific epithelium even after their separation from
473 their *in vivo* tissue microenvironment. Consistent with the concept that, as tissue-resident stem
474 cells, airway BCs regenerate epithelium specific to a region of their residence[13,14,36,52], our study
475 provides evidence for regional memory of BCs in pre-TBs/TBs, the most distal airway segments.
476 BCs isolated from these bronchioles, but not those from proximal airways, were able to generate
477 epithelia with unique cellular composition observed in these distal bronchioles *in vivo*, including
478 the presence of TASCs. This suggests that homeostatic maintenance and repair of the unique
479 epithelial phenotype in pre-TBs/TBs relies on a region-specific regenerative function of resident
480 BCs determined by their regional memory and regulated by their microenvironment.

481 This led us to hypothesize that loss of TASCs, a region-specific differentiation feature of
482 distal airway epithelium in COPD, is due to altered regenerative function of resident BCs. Earlier
483 studies have shown the altered self-renewal and differentiation of BCs from proximal airways of
484 COPD patients[53], and BC clones expanded from COPD lungs can form metaplastic lesions in
485 xenograft models[54]. Based on scRNA-seq data indicating increased $CD8^+$ T cell-driven IFN-γ
486 signaling in COPD distal airway epithelium and expression of IFN-γ receptor genes in BCs, we
487 reasoned that, as a part of the disease-modified niche, IFN-γ may impact the stem cell function of
488 BCs sensing this cytokine. Indeed, we found that IFN-γ, when included in the BC "niche" during
489 their differentiation *in vitro*, suppressed their ability to regenerate TASCs mimicking the altered
490 differentiation pattern observed in distal airway epithelium of COPD patients *in vivo*. This is the
491 first evidence linking T-cell inflammation to altered distal airway regeneration in COPD. The
492 pathophysiological role of other changes in COPD distal airways identified in our study, such as
493 an increased number of mast cells and reduced frequency of capillary endothelial cells, as
494 elements of the disease-modified distal airway microenvironment, requires further investigation.
495 Although functional studies are needed to establish the impact of TASC loss in the lungs
496 of COPD patients on disease evolution, our study suggests that loss of these cells may contribute
497 to altered distal airway homeostasis in this disease. As the major source of surfactant protein
498 expression in this transitional region, where AT2 cells are absent and the airflow pattern shifts
499 from bulk flow characteristic for conducting airways to diffusion in the respiratory zone[55], loss
500 of TASCs may lead to increased surface tension in this region, collapse of peripheral bronchioles
501 during expiration and, thus, contribute to airflow limitation that defines COPD. Further, loss of
502 SCGB3A2, a protein with multiple immunomodulatory and tissue protective properties[56], for
503 which TASCs serve the key source, may facilitate inflammation and contribute to the altered
504 host defense in distal airways in COPD[57], making these airways vulnerable to chronic injury.

505 Suppression of regenerative potential of distal airway BCs due to disease-related changes
506 in their niche may serve as a mechanism of remodeling and loss of distal airways in COPD[4–8]. If
507 so, COPD may represent a disease driven by regenerative failure of distal airways. In support of
508 this concept, previous studies have shown that BCs expanded from small airways or distal lung
509 region of COPD patients fail to establish and maintain mechanically stable, differentiated airway
510 epithelial barrier[58] but instead produce metaplastic pro-inflammatory lesions[54]. In this regard, the
511 pathologic regenerative pattern in COPD distal airways appears remarkably distinct from that
512 observed in idiopathic pulmonary fibrosis (IPF), a disease, in which fibrosis of lung parenchyma
513 is accompanied by the emergence of ectopic bronchiolar epithelium containing BC-like cells[24,59–
514 61] and S-cells, including those expressing TASC markers SCGB3A2 and SFTPB[25]. This suggests
515 the possibility that, similar to distal airway progenitors and bronchoalveolar stem cells in murine
516 lungs[36,62–64], BCs residing in TBs of the human lung, via generation of TASCs, contribute to
517 structural homeostasis in transitional bronchoalveolar segments, RBs, which do not contain BCs
518 or AT2 cells, epithelial progenitors residing in conducting airways and alveoli, respectively[65].
519 Pathologically augmented repair of these segments by distal airway BCs may lead to fibrosis[66],
520 while suppression of this regenerative mechanism may compromise structural integrity of this
521 transitional region and lead to centrilobular emphysema characteristic of COPD[6].
522 Several key aspects of cellular organization of distal airways characterized in this study,
523 including those affected in COPD, are unique to the human lung. Distal airway BCs, epithelial
524 progenitors in this anatomic region in humans, and RBs, transitional bronchoalveolar segments
525 in the human lung, are minimal or absent in commonly used laboratory animals, including the
526 mouse[35,67,68]. A region-precise approach to study cellular organization and regeneration of human
527 distal airways established in our study will facilitate the discovery and pre-clinical targeting of
528 patient-specific mechanisms of distal airway pathology in COPD and other lung diseases.

529 **Authors' contributions**

530 RS: conceived, supervised and supported study

531 SR, SBM: established the methodology of lung tissue dissection, processing and cell isolation

532 SR: performed tissue dissection, immunofluorescence staining and analysis, and *in vitro* studies

533 SR, AFR, RS: performed analysis of immunofluorescence data

534 AFR: performed analysis of imaging mass cytometry (CyTOF) data

535 YH: performed analysis of RNA-seq and scRNA-seq data

536 HR: performed imaging mass cytometry (CyTOF) analysis

537 OE: supervised analysis of RNA-seq, scRNA-seq and imaging CyTOF data

538 SHR, BR, VP, JAK, TSB, FDO: provided lung tissue samples

539 AU: assisted with lung tissue procurement

540 SHR, VP and TSB: provided histological samples for imaging studies

541 FJM: assisted with clinical expertise and resources

542 SR, YH, OE, RS: performed integrated data analysis and interpretation of data

543 RS: wrote the manuscript

544 All authors reviewed and edited the final version of the manuscript.

545

546 **Acknowledgements.** These studies were supported by the National Institutes of Health grants

547 U01 HL145561, R01 HL123544 and R01 HL127393 to RS. We thank personnel of the Marsico

548 Lung Institute Tissue Procurement and Cell Culture Core (supported by Cystic Fibrosis

549 Foundation Grant BOUCHE19R0 and NIH Grant DK065988) for providing lung tissue samples.

550 SBM was supported by the American Lung Association Senior Research Training Fellowship

551 and Weill Cornell Clinical and Translational Science Center TL1 Training Award. AFR is

552 supported by the NCI T32 CA203702 grant. BR was supported by the VA career development

553 grant IK2BX003841. TSB was supported by the VA Merit Review Grant 2 l01 BX002378 to

554 TSB.

Bibliography

1. Haefeli-Bleuer, B. & Weibel, E. R. Morphometry of the human pulmonary acinus. *Anat. Rec.* **220**, 401–414 (1988).

2. Reid, L. The secondary lobule in the adult human lung, with special reference to its appearance in bronchograms. *Thorax* **13**, 110–115 (1958).

3. Webb, W. R. Thin-section CT of the secondary pulmonary lobule: anatomy and the image. *Radiology* **239**, 322–338 (2006).

4. Hogg, J. C. *et al.* The nature of small-airway obstruction in chronic obstructive pulmonary disease. *N. Engl. J. Med.* **350**, 2645–53 (2004).

5. McDonough, J. E. *et al.* Small-airway obstruction and emphysema in chronic obstructive pulmonary disease. *N. Engl. J. Med.* **365**, 1567–75 (2011).

6. Tanabe, N. *et al.* Micro-Computed Tomography Comparison of Preterminal Bronchioles in Centrilobular and Panlobular Emphysema. *Am J Respir Crit Care Med.* **195(5)**, 630–638 (2017).

7. Koo, H. K. *et al.* Small airways disease in mild and moderate chronic obstructive pulmonary disease: a cross-sectional study. *Lancet Respir. Med.* **6**, 591–602 (2018).

8. Tanabe, N. *et al.* Analysis of airway pathology in COPD using a combination of computed tomography, micro-computed tomography and histology. *Eur. Respir. J.* (2018).

9. Galbán, C. J. *et al.* CT-based Biomarker Provides Unique Signature for Diagnosis of COPD Phenotypes and Disease Progression HHS Public Access. *Nat Med* **18**, 1711–1715 (2012).

576 10. Bhatt, S. P. *et al.* Association between functional small airway disease and FEV1 decline
577 in chronic obstructive pulmonary disease. *Am. J. Respir. Crit. Care Med.* **194**, 178–184
578 (2016).

579 11. Vasilescu, D. M. *et al.* Non-Invasive Imaging Biomarker Identifies Small Airway Damage
580 in Severe COPD. *Am. J. Respir. Crit. Care Med.* rccm.201811-2083OC (2019)
581 doi:10.1164/rccm.201811-2083OC.

582 12. Vogelmeier, C. F. *et al.* Global Strategy for the Diagnosis, Management, and Prevention
583 of Chronic Obstructive Lung Disease 2017 Report. GOLD Executive Summary. *Am. J.*
584 *Respir. Crit. Care Med.* **195**, 557–582 (2017).

585 13. Hajj, R. *et al.* Basal cells of the human adult airway surface epithelium retain transit-
586 amplifying cell properties. *Stem Cells* **25**, 139–148 (2007).

587 14. Rock, J. R. *et al.* Basal cells as stem cells of the mouse trachea and human airway
588 epithelium. *Proc. Natl. Acad. Sci. U. S. A.* **106**, 12771–5 (2009).

589 15. Garcıá, S. R. *et al.* Novel dynamics of human mucociliary differentiation revealed by
590 single-cell RNA sequencing of nasal epithelial cultures. *Dev.* **146**, (2019).

591 16. Braga, F. A. V. *et al.* A cellular census of human lungs identifies novel cell states in health
592 and in asthma. *Nat. Med.* (2019).

593 17. Deprez, M. *et al.* A single-cell atlas of the human healthy airways. *Am. J. Respir. Crit.*
594 *Care Med.* **in press**, (2020).

595 18. Montoro, D. T. *et al.* A revised airway epithelial hierarchy includes CFTR-expressing
596 ionocytes. *Nature* **560**, 377–324 (2018).

597 19. Plasschaert, L. W. *et al.* A single-cell atlas of the airway epithelium reveals the CFTR-rich
598 pulmonary ionocyte. *Nature* **560**, 377–381 (2018).

599 20. Widdicombe, J. H. & Wine, J. J. Airway Gland Structure and Function. *Physiol. Rev.* **95**,
600 1241–1319 (2015).

601 21. Hegab, A. E. *et al.* Isolation and in vitro characterization of basal and submucosal gland
602 duct stem/progenitor cells from human proximal airways. *Stem Cells Transl. Med.* **1**, 719–
603 24 (2012).

604 22. Lynch, T. J. *et al.* Submucosal Gland Myoepithelial Cells Are Reserve Stem Cells That
605 Can Regenerate Mouse Tracheal Epithelium. *Cell Stem Cell* **22**, 653-667.e5 (2018).

606 23. Travaglini, K. J. *et al.* A molecular cell atlas of the human lung from single-cell RNA
607 sequencing. *Nature* **587**, 619–625 (2020).

608 24. Adams, T. S. *et al.* Single-cell RNA-seq reveals ectopic and aberrant lung-resident cell
609 populations in idiopathic pulmonary fibrosis. *Sci. Adv.* **6**, 1–17 (2020).

610 25. Habermann, A. *et al.* Single-cell RNA sequencing reveals profibrotic roles of distinct
611 epithelial and mesenchymal lineages in pulmonary fibrosis. *Sci. Adv.* **6**, eaba1972 (2020).

612 26. Gordon, S., Plüddemann, A. & Martinez Estrada, F. Macrophage heterogeneity in tissues:
613 Phenotypic diversity and functions. *Immunol. Rev.* **262**, 36–55 (2014).

614 27. Lavin, Y. *et al.* Tissue-resident macrophage enhancer landscapes are shaped by the local
615 microenvironment. *Cell* **159**, 1312–1326 (2014).

616 28. Jakubzick, C. V., Randolph, G. J. & Henson, P. M. Monocyte differentiation and antigen-
617 presenting functions. *Nat. Rev. Immunol.* (2017) doi:10.1038/nri.2017.28.

618 29. Kumar, B. V., Connors, T. J. & Farber, D. L. Human T Cell Development, Localization,
619 and Function throughout Life. *Immunity* **48**, 202–213 (2018).

620 30. Szabo, P. A. *et al.* Single-cell transcriptomics of human T cells reveals tissue and
621 activation signatures in health and disease. *Nat. Commun.* **10**, (2019).

622 31. Kumar, B. V *et al.* Human Tissue-Resident Memory T Cells Are Defined by Core
623 Transcriptional and Functional Signatures in Lymphoid and Mucosal Sites. *Cell Rep.* **20**,
624 2921–2934 (2017).

625 32. McGinnis, C. S., Murrow, L. M. & Gartner, Z. J. DoubletFinder: Doublet Detection in
626 Single-Cell RNA Sequencing Data Using Artificial Nearest Neighbors. *Cell Syst.* **8**, 329-
627 337.e4 (2019).

628 33. Have-Opbroek, A. A. W. T., Otto-Verberne, C. J. M., Dubbeldam, J. A. & Dÿkman, J. H.
629 The proximal border of the human respiratory unit, as shown by scanning and
630 transmission electron microscopy and light microscopical cytochemistry. *Anat. Rec.* **229**,
631 339–354 (1991).

632 34. Reynolds, S. D., Reynolds, P. R., Pryhuber, G. S., Finder, J. D. & Stripp, B. R.
633 Secretoglobins SCGB3A1 and SCGB3A2 define secretory cell subsets in mouse and
634 human airways. *Am. J. Respir. Crit. Care Med.* **166**, 1498–1509 (2002).

635 35. Rock, J. R., Randell, S. H. & Hogan, B. L. M. Airway basal stem cells: a perspective on
636 their roles in epithelial homeostasis and remodeling. *Dis. Model. Mech.* **3**, 545–556
637 (2010).

638 36. Kumar, P. A. *et al.* Distal airway stem cells yield alveoli in vitro and during lung
639 regeneration following H1N1 influenza infection. *Cell* **147**, 525–538 (2011).

640 37. Fulcher, M. L., Gabriel, S., Burns, K. a, Yankaskas, J. R. & Randell, S. H. Well-
641 differentiated human airway epithelial cell cultures. *Methods Mol. Med.* **107**, 183–206
642 (2005).

643 38. Freeman, C. M. *et al.* Cytotoxic Potential of Lung CD8 + T Cells Increases with Chronic
644 Obstructive Pulmonary Disease Severity and with In Vitro Stimulation by IL-18 or IL-15 .
645 *J. Immunol.* **184**, 6504–6513 (2010).

646 39. Saetta, M. *et al.* CD8+ T-lymphocytes in peripheral airways of smokers with chronic
647 obstructive pulmonary disease. *Am. J. Respir. Crit. Care Med.* **157**, 822–826 (1998).

648 40. Plopper, C. G., Hill, L. H. & Mariassy, A. T. Ultrastructure of the nonciliated bronchiolar
649 epithelial (clara) cell of mammalian lung. III. A study of man with comparison of 15
650 mammalian species. *Exp. Lung Res.* **1**, 171–180 (1980).

651 41. Nakajima, Y. *et al.* Immunohistochemical and ultrastructural studies of basal cells, Clara
652 cells and bronchiolar cuboidal cells in normal human airways. *Pathol. Int.* **48**, 944–953
653 (1998).

654 42. Alon, R. *et al.* Leukocyte trafficking to the lungs and beyond: lessons from influenza for
655 COVID-19. *Nat. Rev. Immunol.* **21**, 49–64 (2021).

656 43. Belvisi, M. G. Overview of the innervation of the lung. *Curr. Opin. Pharmacol.* **2**, 211–
657 215 (2002).

658 44. Wine, J. J. Parasympathetic control of airway submucosal glands: Central reflexes and the
659 airway intrinsic nervous system. *Auton. Neurosci. Basic Clin.* **133**, 35–54 (2007).

660 45. Man, W. H., De Steenhuijsen Piters, W. A. A. & Bogaert, D. The microbiota of the

661 respiratory tract: Gatekeeper to respiratory health. *Nat. Rev. Microbiol.* **15**, 259–270
662 (2017).

663 46. Westphalen, K. *et al.* Sessile alveolar macrophages communicate with alveolar epithelium
664 to modulate immunity. *Nature* **506**, 503–506 (2014).

665 47. Shaykhiev, R. & Crystal, R. G. Early events in the pathogenesis of chronic obstructive
666 pulmonary disease. Smoking-induced reprogramming of airway epithelial basal progenitor
667 cells. *Ann. Am. Thorac. Soc.* **11 Suppl 5**, S252-8 (2014).

668 48. Yang, J. *et al.* Smoking-dependent Distal-to-Proximal Repatterning of the Adult Human
669 Small Airway Epithelium. *Am. J. Respir. Crit. Care Med.* **196**, 340–352 (2017).

670 49. Weibel, E. R. Design of airways and blood vessels considered as branching trees. in *The*
671 *Lung: Scientific Foundations (2nd edition). Philadelphia: Lippincott-Raven Publishers*
672 1061–1071 (1997).

673 50. Shapiro, C. O. *et al.* Airway sensory nerve density is increased in chronic cough. *Am. J.*
674 *Respir. Crit. Care Med.* **203**, 348–355 (2021).

675 51. Allinson, J. P. *et al.* The presence of chronic mucus hypersecretion across adult life in
676 relation to chronic obstructive pulmonary disease development. *Am. J. Respir. Crit. Care*
677 *Med.* **193**, 662–672 (2016).

678 52. Okuda, K. *et al.* Localization of secretory mucins MUC5AC and MUC5B in
679 normal/healthy human airways. *Am. J. Respir. Crit. Care Med.* **199**, 715–727 (2019).

680 53. Ghosh, M. *et al.* Exhaustion of Airway Basal Progenitor Cells in Early and Established
681 COPD. *Am. J. Respir. Crit. Care Med.* **197**, 885–896 (2018).

682 54. Rao, W. *et al.* Regenerative Metaplastic Clones in COPD Lung Drive Inflammation and
683 Fibrosis. *Cell* **181**, 848-864.e18 (2020).

684 55. Hogg, J. C., Paré, P. D. & Hackett, T.-L. The Contribution of Small Airway Obstruction
685 to the Pathogenesis of Chronic Obstructive Pulmonary Disease. *Physiol. Rev.* **97**, 529–552
686 (2017).

687 56. Kimura, S., Yokoyama, S., Pilon, A. L. & Kurotani, R. Emerging role of an
688 immunomodulatory protein secretoglobin 3A2 in human diseases. *Pharmacol. Ther.* **236**,
689 108112 (2022).

690 57. Shaykhiev, R. & Crystal, R. G. Innate immunity and chronic obstructive pulmonary
691 disease: A mini-review. *Gerontology* vol. 59 481–489 (2013).

692 58. Staudt, M. R., Buro-Auriemma, L. J., Walters, M. S. & Salit, J. Airway Basal
693 Stem/Progenitor Cells Have Diminished Capacity to Regenerate Airway Epithelium in
694 Chronic Obstructive Pulmonary Disease. *Am. J. Respir. Crit. Care Med.* **190**, 955–958
695 (2014).

696 59. Kawanami, O., Ferrans, V. J. & Crystal, R. G. Structure of alveolar epithelial cells in
697 patients with fibrotic lung disorders. *Lab Invest* **46**, 39–53 (1982).

698 60. Chilosi, M. *et al.* Abnormal re-epithelialization and lung remodeling in idiopathic
699 pulmonary fibrosis: the role of deltaN-p63. *Lab. Invest.* **82**, 1335–45 (2002).

700 61. Xu, Y. *et al.* Single-cell RNA sequencing identifies diverse roles of epithelial cells in
701 idiopathic pulmonary fibrosis. *JCI Insight* **1**, 214–222 (2016).

702 62. Bender Kim, C. F. *et al.* Identification of bronchioalveolar stem cells in normal lung and

703 lung cancer. *Cell* **121**, 823–835 (2005).

704 63. Zuo, W. *et al.* p63(+)Krt5(+) distal airway stem cells are essential for lung regeneration.
705 *Nature* **517**, 616–620 (2015).

706 64. Vaughan, A. E. *et al.* Lineage-negative Progenitors Mobilize to Regenerate Lung
707 Epithelium after Major Injury. *Nature* **517**, 621–625 (2015).

708 65. Rock, J. R. & Hogan, B. L. Epithelial progenitor cells in lung development, maintenance,
709 repair, and disease. *Annu Rev Cell Dev Biol* **27**, 493–512 (2011).

710 66. Kanegai, C. M. *et al.* Persistent Pathology in Influenza-Infected Mouse Lungs. *Am J*
711 *Respir Cell Mol Biol* **55**, 613–615 (2016).

712 67. Bal, H. S. & Ghoshal, N. G. Morphology of the terminal bronchiolar region of common
713 laboratory mammals. *Lab. Anim.* **22**, 76–82 (1988).

714 68. Basil, M. C. & Morrisey, E. E. Lung regeneration: a tale of mice and men. *Semin. Cell*
715 *Dev. Biol.* **100**, 88–100 (2020).

716

717

718

719

720

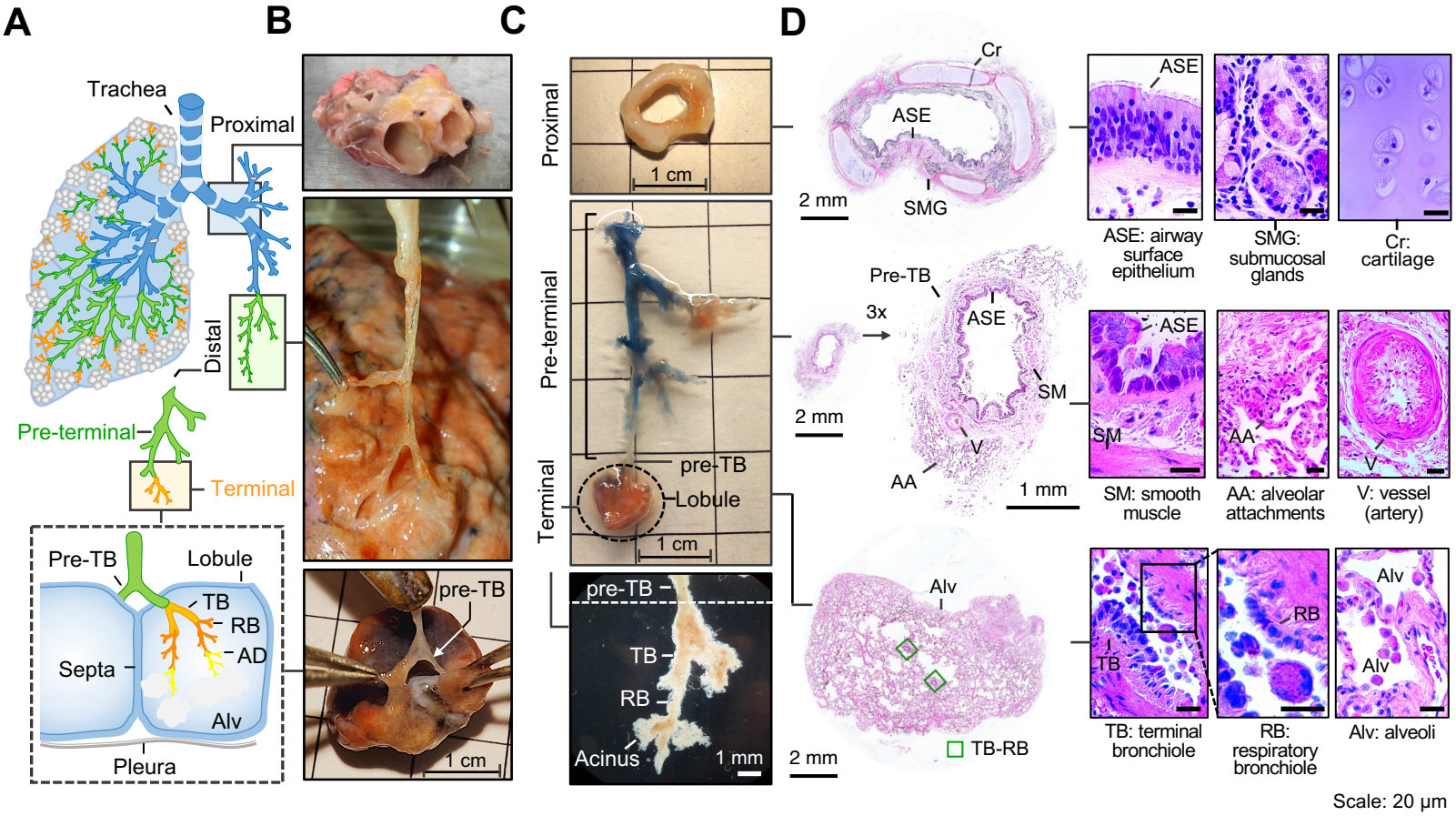
A
B
C
D
Trachea
Proximal
Distal
Pre-terminal
Terminal
Pre-TB
Lobule
TB
RB
AD
Septa
Alv
Pleura
pre-TB
1 cm
Proximal
Pre-terminal
Terminal
pre-TB
Lobule
TB
RB
Acinus
1 mm
Cr
ASE
SMG
2 mm
Pre-TB
3x
SM
V
AA
1 mm
Alv
TB-RB
ASE: airway surface epithelium
SMG: submucosal glands
Cr: cartilage
SM: smooth muscle
AA: alveolar attachments
V: vessel (artery)
TB: terminal bronchiole
RB: respiratory bronchiole
Alv: alveoli
Scale: 20 µm

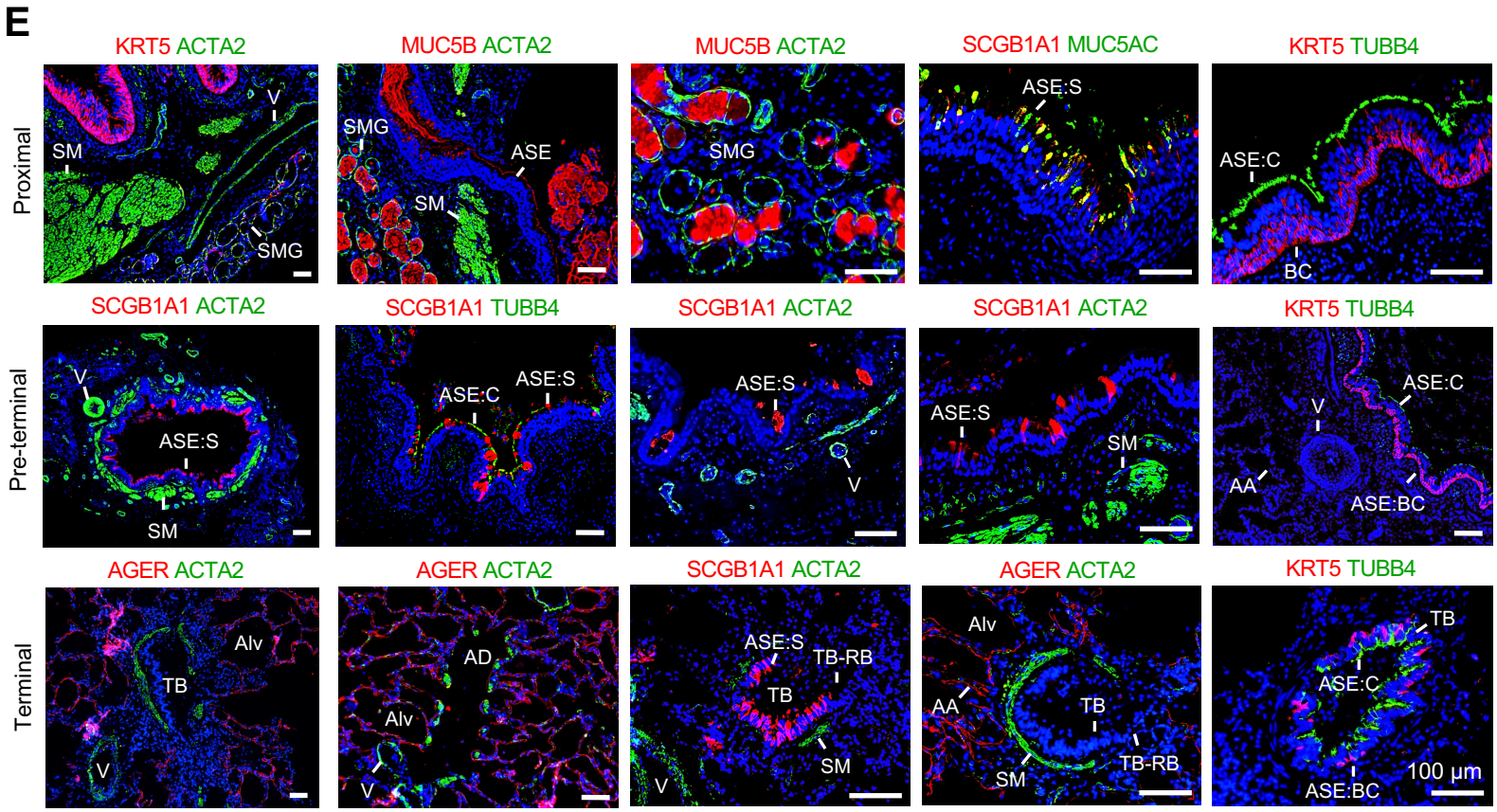
E
KRT5 ACTA2
MUC5B ACTA2
MUC5B ACTA2
SCGB1A1 MUC5AC
KRT5 TUBB4
Proximal
SM
V
SMG
ASE
ASE:S
ASE:C
BC
SCGB1A1 ACTA2
SCGB1A1 TUBB4
SCGB1A1 ACTA2
SCGB1A1 ACTA2
KRT5 TUBB4
Pre-terminal
ASE:S
SM
ASE:C
V
AA
ASE:BC
AGER ACTA2
AGER ACTA2
SCGB1A1 ACTA2
AGER ACTA2
KRT5 TUBB4
Terminal
Alv
TB
AD
TB-RB
100 µm

Figure 1. Anatomical landmarking and region-precise dissection of human distal airways.

A. The human respiratory tree is composed of proximal (P; blue; trachea and cartilaginous bronchi) and distal (bronchioles, diameter < 2 mm) airways. The distal airway dissection method in our study regards pre-terminal bronchioles (pre-TBs), the last macroscopically visible segments in the bronchial pathway, that lead to secondary pulmonary lobules ("lobules"), as a boundary between pre-terminal (pre-T; green) and terminal (T; orange) airway regions. Pre-T region included pre-lobular bronchioles (pre-TBs and 3-4 generations proximal to pre-TBs). T-region included intralobular segments distal to visible parts of pre-TBs (terminal bronchioles [TBs], respiratory bronchioles [RBs], alveolar ducts [ADs] and alveoli [Alv]).

B. Examples of samples used for dissection of P **(upper)**, pre-T **(middle)**, and T (**lower**; pre-TBs leading to lobules are indicated) regions.

C. Example of dissected regions: P **(upper)**, pre-T and T **(middle**; T-region, represented by lobule, is outlined by dashed line; pre-TB marking the boundary between pre-T and T regions is indicated**)**; **lower:** T-region inspected under tissue dissection microscope (shows intralobular segments distal to pre-TBs: TBs, RBs and alveolar tissue descending from RBs that constitute pulmonary acinus).

D. Hematoxylin and eosin staining of representative dissected P, pre-T and T regions; major histological landmarks are shown.

E. Immunofluorescence staining of dissected P, pre-T and T regions shown in **D**; histological landmarks are labeled as described in **D**; antibodies used to mark specific cell types: KRT5 (keratin 5; basal cells [BCs]), SCGB1A1 (secretoglobin 1A1; secretory cells [S]), mucins MUC5AC (mucus-producing S-cells of airway surface epithelium [ASE]) and MUC5B (mucinous S-cells of submucosal glands [SMG] and ASE), TUBB4 (tubulin, β4; cilia/ciliated [C] cells of ASE); ACTA2 (α-smooth muscle actin; smooth muscle [SM]); AGER (alveolar type 1 [AT1] cells; alveolar epithelium).

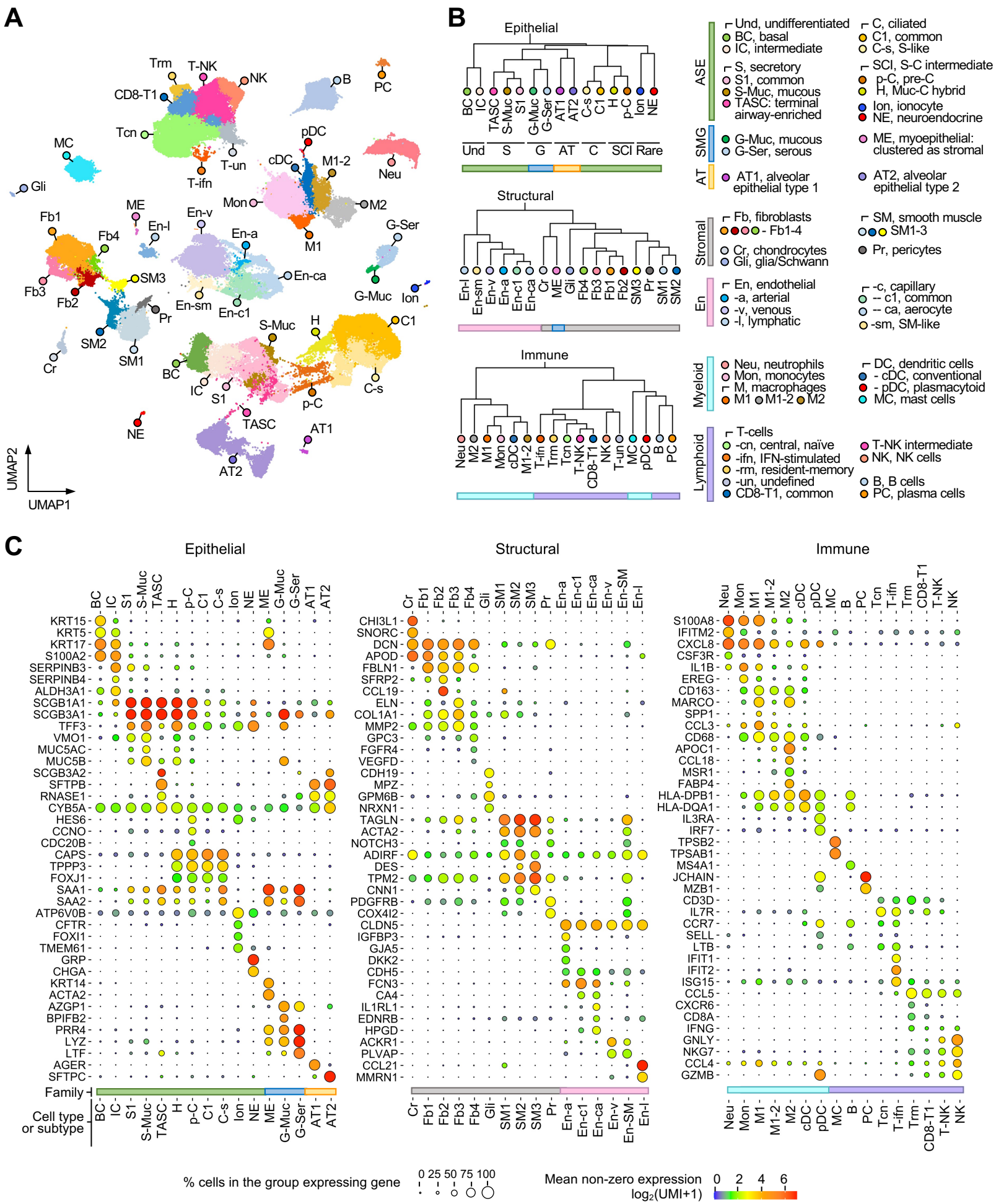
A
Trm
T-NK
NK
B
PC
CD8-T1
Tcn
MC
T-un
T-ifn
pDC
cDC
M1-2
Neu
Gli
Mon
M2
ME
En-v
En-l
En-a
G-Ser
Fb1
Fb4
M1
SM3
En-ca
Fb3
Fb2
En-sm
En-c1
G-Muc
Ion
Pr
S-Muc
H
C1
SM2
SM1
Cr
BC
IC
S1
C-s
p-C
NE
TASC
AT1
AT2
UMAP2
UMAP1
B
Epithelial
BC IC TASC S-Muc S1 G-Muc G-Ser AT1 AT2 C-s C1 H p-C Ion NE
Und S G AT C SCI Rare
Structural
En-l En-sm En-v En-a En-c1 En-ca Cr ME Gli Fb4 Fb3 Fb1 Fb2 SM3 Pr SM1 SM2
Immune
Neu M2 M1 Mon cDC M1-2 T-ifn Trm Tcn T-NK CD8-T1 NK T-un MC pDC B PC
ASE
Und, undifferentiated
BC, basal
IC, intermediate
S, secretory
S1, common
S-Muc, mucous
TASC: terminal airway-enriched
C, ciliated
C1, common
C-s, S-like
SCI, S-C intermediate
p-C, pre-C
H, Muc-C hybrid
Ion, ionocyte
NE, neuroendocrine
SMG
G-Muc, mucous
G-Ser, serous
ME, myoepithelial: clustered as stromal
AT
AT1, alveolar epithelial type 1
AT2, alveolar epithelial type 2
Stromal
Fb, fibroblasts
Fb1-4
Cr, chondrocytes
Gli, glia/Schwann
SM, smooth muscle
SM1-3
Pr, pericytes
En
En, endothelial
-a, arterial
-v, venous
-l, lymphatic
-c, capillary
-- c1, common
-- ca, aerocyte
-sm, SM-like
Myeloid
Neu, neutrophils
Mon, monocytes
M, macrophages
M1 M1-2 M2
DC, dendritic cells
- cDC, conventional
- pDC, plasmacytoid
MC, mast cells
Lymphoid
T-cells
-cn, central, naïve
-ifn, IFN-stimulated
-rm, resident-memory
-un, undefined
CD8-T1, common
T-NK intermediate
NK, NK cells
B, B cells
PC, plasma cells
C
Epithelial
BC IC S1 S-Muc TASC H p-C C1 C-s Ion NE ME G-Muc G-Ser AT1 AT2
KRT15 KRT5 KRT17 S100A2 SERPINB3 SERPINB4 ALDH3A1 SCGB1A1 SCGB3A1 TFF3 VMO1 MUC5AC MUC5B SCGB3A2 SFTPB RNASE1 CYB5A HES6 CCNO CDC20B CAPS TPPP3 FOXJ1 SAA1 SAA2 ATP6V0B CFTR FOXI1 TMEM61 GRP CHGA KRT14 ACTA2 AZGP1 BPIFB2 PRR4 LYZ LTF AGER SFTPC
Family
Cell type or subtype
Structural
Cr Fb1 Fb2 Fb3 Fb4 Gli SM1 SM2 SM3 Pr En-a En-c1 En-ca En-v En-SM En-l
CHI3L1 SNORC DCN APOD FBLN1 SFRP2 CCL19 ELN COL1A1 MMP2 GPC3 FGFR4 VEGFD CDH19 MPZ GPM6B NRXN1 TAGLN ACTA2 NOTCH3 ADIRF DES TPM2 CNN1 PDGFRB COX4I2 CLDN5 IGFBP3 GJA5 DKK2 CDH5 FCN3 CA4 IL1RL1 EDNRB HPGD ACKR1 PLVAP CCL21 MMRN1
Immune
Neu Mon M1 M1-2 M2 cDC pDC MC B PC Tcn T-ifn Trm CD8-T1 T-NK NK
S100A8 IFITM2 CXCL8 CSF3R IL1B EREG CD163 MARCO SPP1 CCL3 CD68 APOC1 CCL18 MSR1 FABP4 HLA-DPB1 HLA-DQA1 IL3RA IRF7 TPSB2 TPSAB1 MS4A1 JCHAIN MZB1 CD3D IL7R CCR7 SELL LTB IFIT1 IFIT2 ISG15 CCL5 CXCR6 CD8A IFNG GNLY NKG7 CCL4 GZMB
% cells in the group expressing gene
0 25 50 75 100
Mean non-zero expression
log2(UMI+1)
0 2 4 6

Figure 2. Single-cell RNA-seq analysis of cellular diversity along the bronchoalveolar axis.

A. Uniform manifold approximation and projection (UMAP) clustering of 111,744 single cells isolated from proximal (P; n=5), pre-terminal (pre-T; n=13) and terminal regions (T; n=7) of normal lungs and pre-T airways of COPD subjects (n=5).

B. Dendrograms showing hierarchical clustering of cell groups identified in **A** based on top 2000 variable genes using Spearman correlation and complete linkage algorithm: three large clusters representing epithelial, non-epithelial structural ("structural") and hematopoietic/immune ("immune") cell superfamilies are shown as separate dendrograms; cell groups are listed.

C. Dot-plots showing expression of selected marker genes in indicated cell groups; dot size reflects percentage of cells within a group expressing given gene; dot color shows mean expression level as indicated.

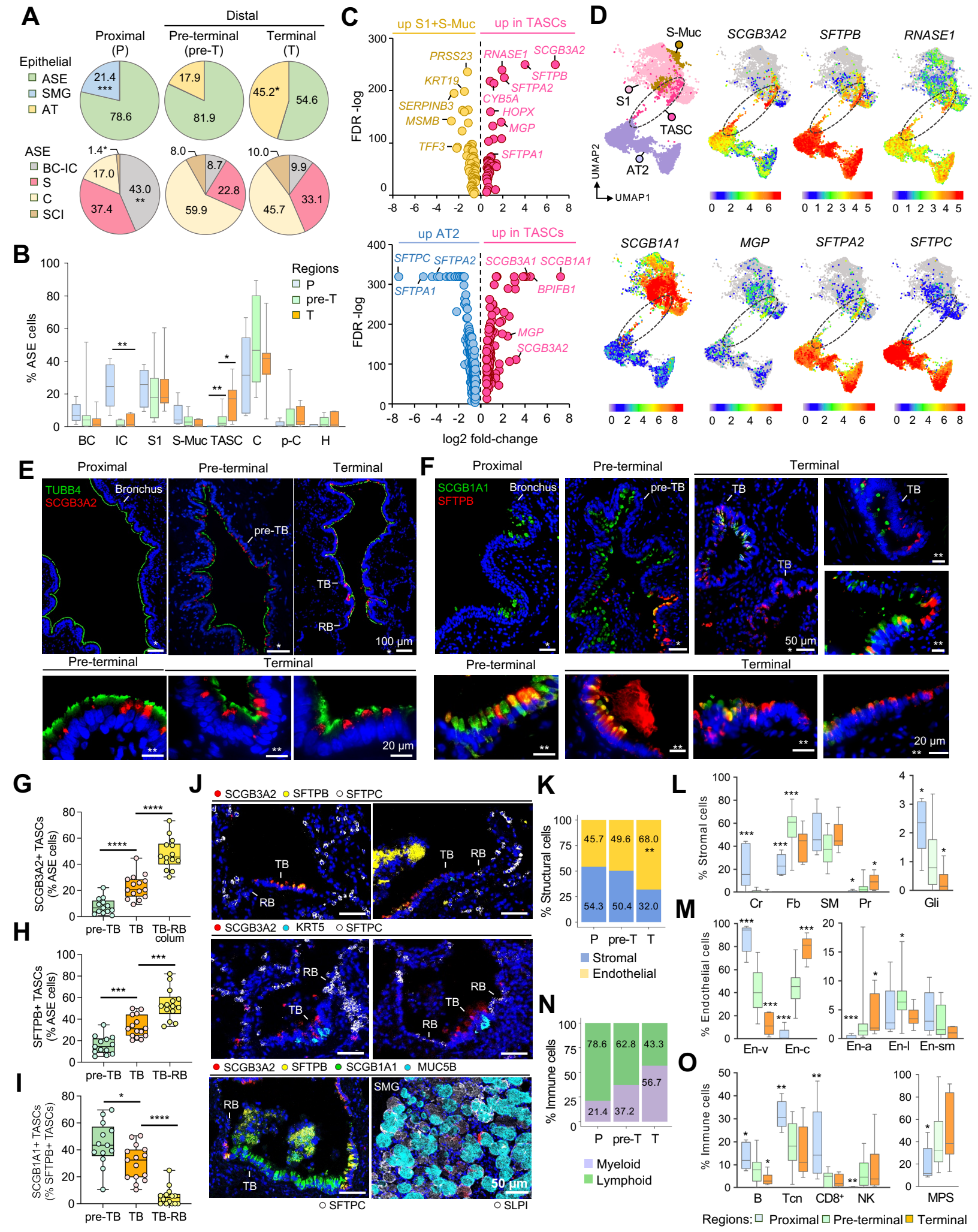
A
Proximal (P)
Distal
Pre-terminal (pre-T)
Terminal (T)
Epithelial
ASE
SMG
AT
21.4 ***
78.6
17.9
81.9
45.2*
54.6
ASE
BC-IC
S
C
SCI
1.4*
17.0
43.0 **
37.4
8.0
8.7
22.8
59.9
10.0
9.9
33.1
45.7
B
% ASE cells
Regions
P
pre-T
T
BC
IC
S1
S-Muc
TASC
C
p-C
H
C
up S1+S-Muc
up in TASCs
FDR -log
PRSS23
KRT19
SERPINB3
MSMB
TFF3
RNASE1
SCGB3A2
SFTPB
SFTPA2
CYB5A
HOPX
MGP
SFTPA1
up AT2
up in TASCs
SFTPC
SFTPA2
SFTPA1
SCGB3A1
SCGB1A1
BPIFB1
MGP
SCGB3A2
log2 fold-change
D
S-Muc
S1
TASC
AT2
UMAP2
UMAP1
SCGB3A2
SFTPB
RNASE1
SCGB1A1
MGP
SFTPA2
SFTPC
E
Proximal
Pre-terminal
Terminal
TUBB4
SCGB3A2
Bronchus
pre-TB
TB
RB
100 µm
20 µm
F
Proximal
Pre-terminal
Terminal
SCGB1A1
SFTPB
Bronchus
pre-TB
TB
50 µm
20 µm
G
SCGB3A2+ TASCs (% ASE cells)
pre-TB
TB
TB-RB colum
H
SFTPB+ TASCs (% ASE cells)
pre-TB
TB
TB-RB
I
SCGB1A1+ TASCs (% SFTPB+ TASCs)
pre-TB
TB
TB-RB
J
SCGB3A2
SFTPB
SFTPC
TB
RB
SCGB3A2
KRT5
SFTPC
SCGB3A2
SFTPB
SCGB1A1
MUC5B
SMG
50 µm
SFTPC
SLPI
K
% Structural cells
45.7
49.6
68.0 **
54.3
50.4
32.0
P
pre-T
T
Stromal
Endothelial
N
% Immune cells
78.6
62.8
43.3
56.7
21.4
37.2
P
pre-T
T
Myeloid
Lymphoid
L
% Stromal cells
Cr
Fb
SM
Pr
Gli
M
% Endothelial cells
En-v
En-c
En-a
En-l
En-sm
O
% Immune cells
B
Tcn
CD8+
NK
MPS
Regions: Proximal Pre-terminal Terminal

Figure 3. Region-specific cellular heterogeneity along the bronchoalveolar axis.

A. Proportions (%) of cells belonging to indicated families based on scRNA-seq data described in **Fig. 2** (see details in **Table S3**) within epithelial superfamily (**upper;** ASE; airway surface epithelium; SMG; submucosal gland; AT; alveolar epithelium): average % of cells per sample in indicated regions of non-diseased lungs: 5 proximal, 13 pre-terminal, 7 terminal samples); and in ASE family (**lower;** BC-IC, undifferentiated [basal and intermediate], S, secretory [S1 common S, S-Muc, mucous; TASCs, terminal airway-enriched S], C, ciliated [C1, common, and C-s, S-like], SCI, S-C intermediate [H, hybrid; p-C, pre-ciliated] cells;

B. Average % of cells belonging to indicated cell types (per sample; as described in **A**) within ASE family in different regions;

C. Volcano plots (based on scRNA-seq data shown in **Fig. 2**): differentially expressed genes (DEGs) identified by comparing all: **(upper)** TASCs and other S (S1 and S-Muc) cells; **(lower)** TASCs and AT type 2 (AT2) cells; shown DEGs with FDR <0.01 and log2FC >0.5 or < -0.5.

D. Portion of the UMAP graph showed in **Fig. 2A** including only S1, S-Muc, TASC and AT2 cells. A clustering region, where TASCs are enriched and form a bridge between S- and AT2 cells, is demarcated (dashed line). Expression of selected DEGs identified in the analysis shown in **C** is color-mapped (see scale bar for expression levels).

E, F. Immunofluorescence (IF) images showing expression of **E:** secretoglobin 3A2 (SCGB3A2) and tubulin beta 4 (TUBB4; cilia marker); **F:** surfactant protein B (SFTPB) and SCGB1A1 (S1-cell marker) in indicated regions;

G-I. % of **G:** SCGB3A2$^+$ TASCs; **H:** SFTPB$^+$ TASCs among ASE cells, and **I**: SCGB1A1$^+$ cells among SFTPB$^+$ TASCs in indicated regions; TB-RB: simple epithelium (colum, columnar) in TB-RB transition areas.

J. Representative CyTOF images showing expression of indicated markers in different regions;

K. Proportions of structural cell families (average % cells per sample) in different regions;

L, M. Average % of indicated cell types (per sample; as described in **A**; cell type names as described in **Fig. 2B**) within stromal **(L)** and endothelial (En; **M**) cell families;

N. Proportions of cell representing immune families (average % cells per sample) in different regions;

O. Average proportions of indicated cell types (per sample; as described in **A**; cell type names as described in **Fig. 2B**) in different regions.

In **A, B, G-I, K-O**: *p<0.05, **p<0.01; ***p<0.005; ****p<0.0001 (two-tailed Mann-Whitney test) *vs* other or indicated regions.

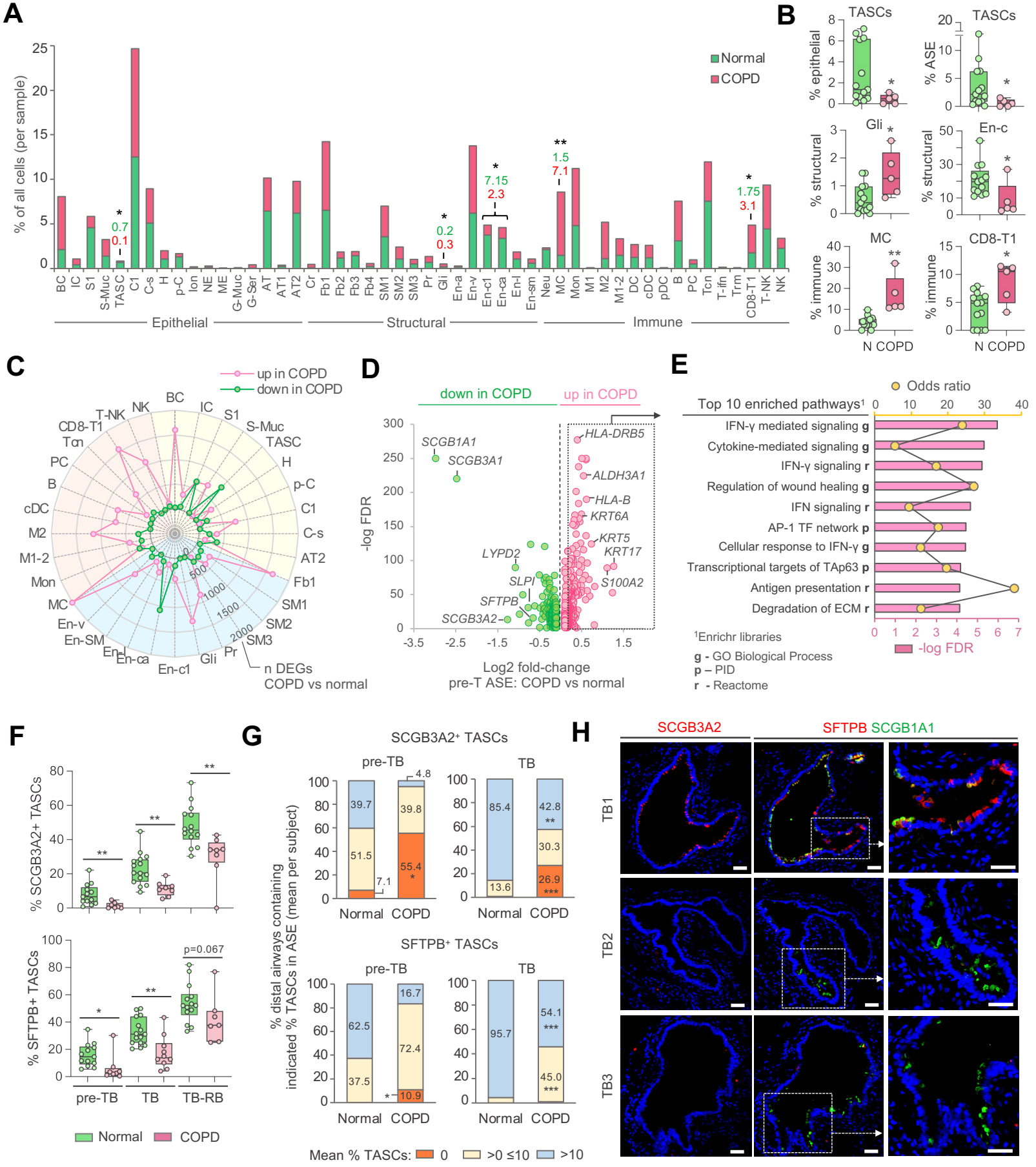
A
% of all cells (per sample)
Normal
COPD
Epithelial
Structural
Immune
B
TASCs
% epithelial
% ASE
Gli
En-c
% structural
MC
CD8-T1
% immune
N COPD
C
up in COPD
down in COPD
n DEGs
COPD vs normal
D
down in COPD
up in COPD
-log FDR
SCGB1A1
SCGB3A1
HLA-DRB5
ALDH3A1
HLA-B
KRT6A
KRT5
KRT17
S100A2
LYPD2
SLPI
SFTPB
SCGB3A2
Log2 fold-change
pre-T ASE: COPD vs normal
E
Odds ratio
Top 10 enriched pathways[1]
IFN-γ mediated signaling g
Cytokine-mediated signaling g
IFN-γ signaling r
Regulation of wound healing g
IFN signaling r
AP-1 TF network p
Cellular response to IFN-γ g
Transcriptional targets of TAp63 p
Antigen presentation r
Degradation of ECM r
-log FDR
[1]Enrichr libraries
g - GO Biological Process
p – PID
r - Reactome
F
% SCGB3A2+ TASCs
% SFTPB+ TASCs
p=0.067
pre-TB
TB
TB-RB
Normal
COPD
G
SCGB3A2+ TASCs
SFTPB+ TASCs
pre-TB
TB
% distal airways containing indicated % TASCs in ASE (mean per subject)
Normal
COPD
Mean % TASCs: 0 >0 ≤10 >10
H
SCGB3A2
SFTPB SCGB1A1
TB1
TB2
TB3

Figure 4. Changes in cellular organization of distal airways in COPD.

A, B. scRNA-seq analysis- based proportions of indicated cell types and subtypes (abbreviations as described in **Fig. 2B**) in pre-terminal (pre-T) airway samples of donors without lung disease ("normal"; n=13) and those from subjects with COPD (n=5): **A.** Mean percentage (%) of cells in indicated cell groups among all single cells per sample (values are shown for cell groups with significant differences between the groups; green, normal; pink, COPD); **B.** Mean % of cells in indicated cell groups among all single cells per sample within corresponding superfamilies (dots: individual samples).

C. Radar plot showing numbers of differentially expressed genes (DEGs) identified by comparing scRNA-seq average gene expression profiles of indicated cell types/subtypes in pre-T samples (COPD *vs* normal) described in **A-B**. Criteria for cell type/subtype inclusion: >10 cells per group (normal; COPD) and at least 3 cells in >50% samples in each group. Colored areas - epithelial (yellow), structural (blue), and immune (red) cell superfamilies. Dots show numbers of DEGs up- (pink) or down-regulated (green) in COPD *vs* normal samples (Mann-Whitney $p<0.05$).

D. Volcano plot showing DEGs (FDR <0.05) identified by comparison of scRNA-seq average expression profiles of airway surface epithelial (ASE) cells in COPD *vs* normal pre-T samples (described in **A-B**).

E. Top 10 annotation categories (pathways) among Gene Ontology (GO) Biological Process; Reactome and NCI-Nature Pathway Interaction database (PID) libraries identified as enriched in DEGs up-regulated in ASE of COPD pre-T *vs* ASE of normal pre-T samples (log2 fold-change >0.2; dashed box in **D**); ranked by -log FDR of enrichment; dots - odds ratio of enrichment based on Enrichr analysis.

F-H. IF analysis: **F.** mean % of SCGB3A2$^+$ **(upper)** and SFTPB$^+$ **(lower)** TASCs per subject among ASE cells in pre-TB, TB, and TB-RB (defined as in **Fig. 3G-I**) of normal lung donors (green) and COPD subjects (pink); dots represent individual subjects (see **Table S5** for details). **G.** Distribution of distal airways (pre-TBs and TBs) in normal and COPD lung tissue samples (described in **F**) based on average % of SCGB3A2$^+$ **(upper)** and SFTPB$^+$ **(lower)** cells in ASE of these airways (per subject); in **A**, **B**, **F** and **G**: *$p<0.05$, **$p<0.01$; ***$p<0.005$ (two-tailed Mann-Whitney test) comparing COPD vs normal. **H.** Representative IF images showing SCGB3A2$^+$ TASCs (left), SFTPB$^+$ TASCs and SCGB1A1 expression (right) in different TBs of the same COPD patient's lung; scale bars: 50 μm.

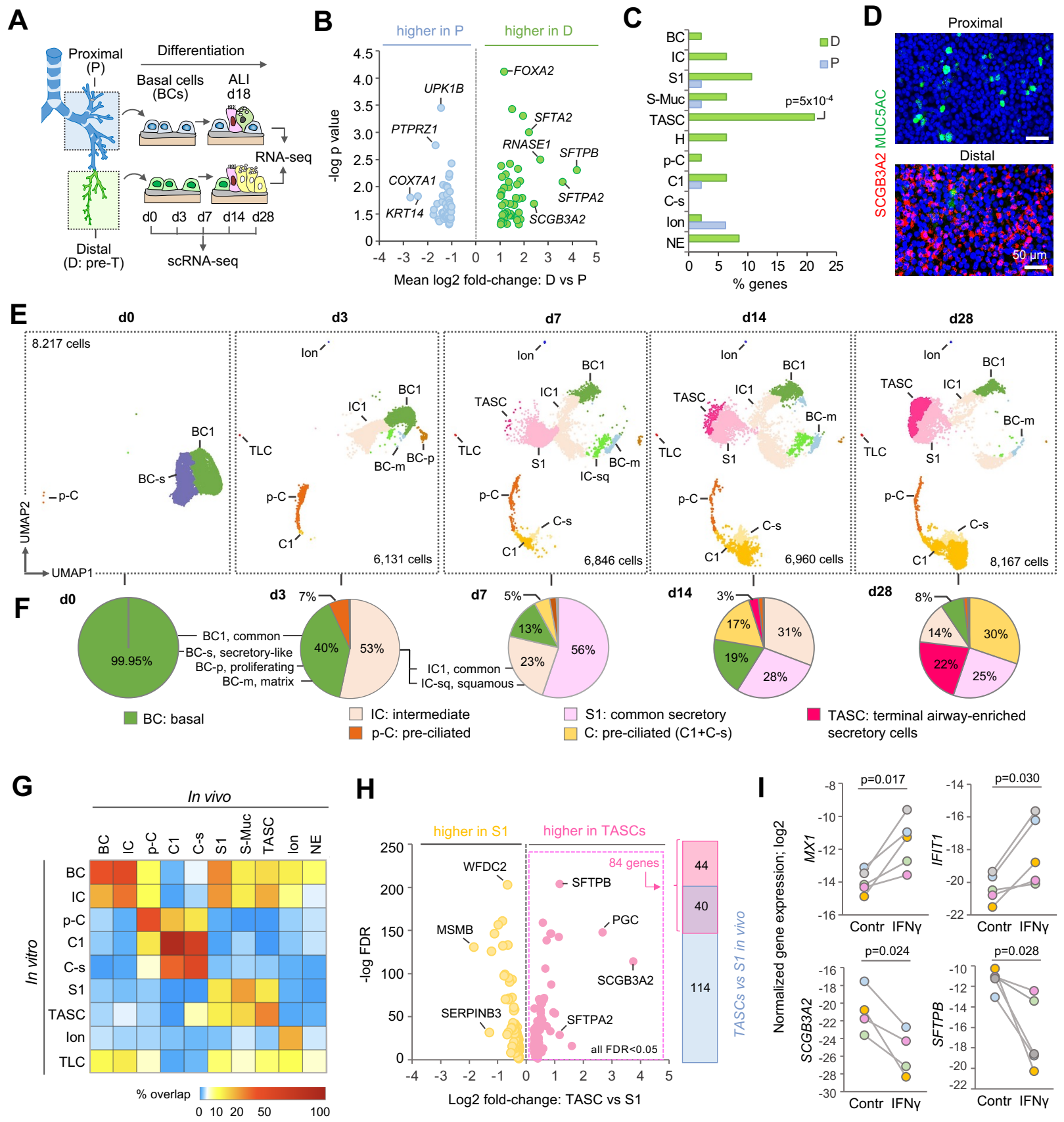
A
Proximal (P)
Differentiation
Basal cells (BCs)
ALI d18
RNA-seq
d0 d3 d7 d14 d28
Distal (D: pre-T)
scRNA-seq
B
higher in P
higher in D
-log p value
UPK1B
PTPRZ1
COX7A1
KRT14
FOXA2
SFTA2
RNASE1
SFTPB
SFTPA2
SCGB3A2
Mean log2 fold-change: D vs P
C
BC
IC
S1
S-Muc
TASC
H
p-C
C1
C-s
Ion
NE
D
P
p=5x10-4
% genes
D
Proximal
Distal
SCGB3A2 MUC5AC
50 µm
E
d0
d3
d7
d14
d28
8,217 cells
6,131 cells
6,846 cells
6,960 cells
8,167 cells
UMAP2
UMAP1
F
99.95%
BC1, common
BC-s, secretory-like
BC-p, proliferating
BC-m, matrix
7%
40%
53%
5%
13%
23%
56%
IC1, common
IC-sq, squamous
3%
17%
19%
28%
31%
8%
14%
22%
25%
30%
BC: basal
IC: intermediate
p-C: pre-ciliated
S1: common secretory
C: pre-ciliated (C1+C-s)
TASC: terminal airway-enriched secretory cells
G
In vivo
In vitro
% overlap
0 10 20 50 100
H
higher in S1
higher in TASCs
-log FDR
WFDC2
MSMB
SERPINB3
SFTPB
PGC
SCGB3A2
SFTPA2
84 genes
all FDR<0.05
44
40
114
TASCs vs S1 in vivo
Log2 fold-change: TASC vs S1
I
Normalized gene expression; log2
MX1
IFIT1
SCGB3A2
SFTPB
p=0.017
p=0.030
p=0.024
p=0.028
Contr IFNγ

Figure 5. Distal airway basal cells (BCs) as the cellular origin of terminal airway-enriched secretory cells (TASCs).

A. Design of *in vitro* studies. BCs isolated from proximal (P) and distal (D; pre-terminal [pre-T] region) were cultured under the same conditions in the transwell system. After BCs established confluent layer, apical media was removed to establish air-liquid interface (ALI) and media was supplied only via the basolateral side. At indicated time-points of ALI culture representing different stages of BC differentiation samples were analyzed.

B. Volcano plot showing differentially expressed genes (DEGs) identified by comparison of transcriptomes of ALI-day 18 epithelia generated by BCs isolated from P- and D-airways of 6 donors without lung disease (shown DEGs with log2 FC >1, 2-tailed paired t-test $p<0.05$).

C. Proportions (%) of DEGs up-regulated in ALI-day 18 ASE generated by BCs from matched P (blue) and D (green) airways (described in **B**) overlapping with marker genes of indicated pre-T ASE cell types based on scRNA-seq analysis (criteria: log2FC >1; FDR<0.05).

D. Immunofluorescence staining of ALI-day 18 membranes showing apical surface of epithelia generated by BCs from P- (upper) and D- (lower) airways; red: secretoglobin SCGB3A2, green: mucin MUC5AC; blue: DAPI.

E. UMAP clustering of cells at indicated time-points of ALI culture of the same distal airway BC sample; total number of single cells captured in each time-point is indicated.

F. % of cell types at ALI time-points shown in **E**. TLCs, tuft-like cells.

G. Heatmap: % DEGs of indicated ASE cell types *in vivo* overlapping with those identified for cell types in ALI-day 28 epithelia derived from D-airway BCs shown in **E** using the same criteria: FDR<0.05; log2 fold-change >0.5 *vs* other ASE cells.

H. Volcano plot: DEGs (FDR <0.05) identified by comparison of TASCs and S1-cells in ALI-day 28 epithelia generated by D-airway BCs (shown in **E**); right side: overlap between DEGs up-regulated in TASCs *vs* S1 *in vitro* and those identified in the same comparison *in vivo*.

I. log2 normalized expression of indicated genes in ALI-day 18-40 epithelia generated by distal airway BCs in the presence or absence of 5 ng/ml IFN-γ; dot colors mark independent samples; p values based on 2-tailed paired t-test; see details in **Fig. S9D**.